Journal of Inorganic and General Chemistry
ZAAC
Zeitschrift für anorganische und allgemeine Chemie
www.zaac.wiley-vch.de
REVIEW
Check for updates
DOI: 10.1002/zaac.202400011

A Review on Binary Alkaline-Earth Trielides: an Overview of Compositions and Structures, of their Stabilities and Energetics and of Criteria for the Validity of the Zintl-Concept

Horst P. Beck*[a]

In recognition of the outstanding scientific achievements by Eduard Zintl on the occasion of his 125th birthday

Omitting alloys with a compositional range we present a compilation of binary alkaline earth trielides AE_xTR_y together with results of DFT calculations to estimate total energies and energies of formation in comparison and to analyse the distribution of charges at the atomic positions in a Bader analysis of the electron density. In a comparison of many structures, we furthermore analyse the effect of bonding on this charge distribution and reflect on the real bonding patterns in comparison with our expectations according to the Zintl concept, and we find mechanisms blocking an electron transfer as favoured by the electronegativity differences. We have subjected a variety of structural parameters together with the DFT results to a Principal Component Analysis to explore their relationship which we describe in the form of correlation matrices and biplots. The Zintl rules turn out to be a very slack guideline in rationalizing the structures of these compounds.

Introduction

There have been many attempts to describe and rationalize the chemistry, structure, and bonding of Zintl-phases and -ions.[1,2,3] The Zintl-concept has proven to be a valuable means of understanding the great variety of structures in a large group of intermetallic compounds where we focus not only on the geometry of primary coordination of oppositely charged ions but rather on the topology of homonuclear contacts. It is then a task to evaluate and understand the nature of such contacts in terms of chemical bonds and to analyse the topology of bond nets and its importance for the stabilization of the individual structures. The group of binary alkaline earth trielides (AE_xTR_y), chosen here, offers a good compendium of many variants of structures where this concept may hold and presents a field for deeper exploration.

In this paper we present a compilation of such compounds found in data bases.[4a,b] We have omitted alloys whith a compositional range – as often found for Mg-aluminides – or examples with partial occupancy of sites and statistical distribution of different atoms, and we have let aside borides which have their own field of structures and bonding. This has left us with about 90 cases to study the structures and to apply DFT calculations to elucidate their energetics and to depict the respective electron distribution in space. Finally, we have subjected various parameters resulting from such calculations and associated with the formation of certain structures and various types of bonding in these compounds to a multivariate analysis to elucidate correlations and "causes" for hits or misses in the frame of the Zintl concept.

Figure 1 gives an overview of all our examples in elemental groups together with the relative contents of the alkaline-earth partner which turns out to be a decisive parameter in all facets of the study.

Across all elemental combinations we find frequent simple stoichiometric relations, but also unique compositions realized only for a single element pair. The importance and stability of such frequent compositions is very often documented in the corresponding AE-TR-phase diagrams where they usually stand out as stable phases. According to the Zintl-concept the relative AE-content of about 0.7 would be the highest one up to which we may expect TR-TR-bonds since this would then mark the TR atom as a ψ-halogen exerting only one bond to its homologous neighbour. Lower values should give rise to more bonds. However, we will see in the following that such counting-out rhymes do not always hold.

In the following we first present the results of DFT calculations in several tables (Table 1) (Table 2–4 in the electronic supplementary information (ESI)) where we give the space groups and the DFT-optimized lattice parameters of all compounds together with the Wyckoff positions of the atoms, the respective Bader charges and basin volumes and the number of bonds of the trielide partners. The tables also

[a] *H. P. Beck*
Institut für Anorganische und Analytische Chemie der Universität des Saarlandes
Campus Dudweiler Beethovenstraße Zeile 4, D-66125 Saarbrücken
E-mail: hp.beck@mx.uni-saarland.de

Supporting information for this article is available on the WWW under https://doi.org/10.1002/zaac.202400011

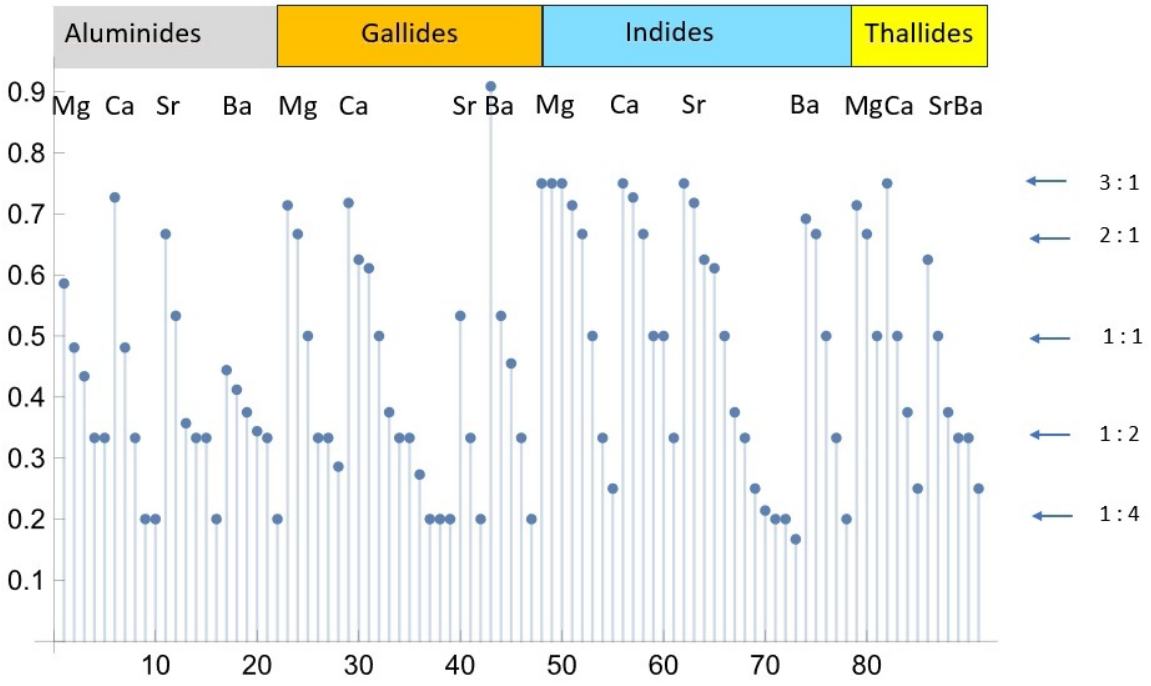

Figure 1. Relative Alkaline-earth content grouped according to the elemental combinations in our list of compounds. (The specific pattern in this presentation arises from the sequence of grouping which we have chosen for all tables in this paper. We always start with the highest AE-content, and we list in decreasing order).

contain energies per atom and formation enthalpies for a comparison of the relative stability of different compounds by a presentation of so-called hull curves.

We discuss the development of charges and basin volumes in the context of the bonding of the anionic partners, and we venture to describe the causal connections within the "charge – bond number – volume" triple in a comparison of structures. We then present the variations in bonding which occur in closely related structures and describe their relationship in terms of group-subgroup notations in Bärnighausen trees.[6,7] Finally, we probe this complex data set by a multivariate analysis hoping to find hidden correlations and hints for a deeper insight into the mechanisms governing this dazzling variety of compounds and structures.

Calculation Procedures

Electronic structure calculations of the AE_xTR_y compounds were performed using the projector augmented wave method (PAW) of Blöchl[8,9] coded in the Vienna ab initio simulation package (VASP).[10,11] VASP calculations employed the potentials PAW_PBE Mg 13Apr2007, PAW_PBE Ca 06Sep2000, PAW_PBE Sr_sv 07Sep2000, PAW_PBE Ba sv 06Sep2000 and PAW_PBE Al 04Jan2000, PAW_PBE Ga 06Jul2010, PAW_PBE In 08Apr2002, PAW_PBE Tl 02Apr2002. Runs using the generalized gradient approximation (GGA) with exchange and correlation treated by Perdew-Burke-Enzerhof (PBE)[12] for comparison did not result in significant changes. The cutoff energy for the plane wave calculations was set to 550 eV and the Brillouin zone integration was carried out using an automated Γ-centred 20-fold *k*-point mesh. The Bader charge analysis was based on VASP outputs with subsequent calculations with the Bader program developed by the Henkelman group.[13–15] All calculations could of course be done on more sophisticated levels, and for Thallium compounds relativistic approaches would certainly be worthwhile. However, we have abstained from doing so in order to have a comparable treatment for the whole set of compounds. Calculations on higher levels may give slightly different energies and electron densities, however, we are convinced that the overall picture and the relations of all calculated parameters would be essentially the same.

As starting point for our calculations, we have used the crystallographic data given in the Pearson[4a] and ICSD[4b] databases. For the multivariate analysis we have chosen the PCA package of Origin®. Calculations of the Madelung Part of Lattice Energy (MAPLE) have been done according to the Ewald-Bertaut method using an inhouse programme (COUPOT).[5]

On the Energetics of AE_xTR_y Compounds

We have assembled the results of our DFT calculations in several tables giving structural parameters, Bader charges, basin volumes and energies per atom. Table 1 (and Table S1 in the electronic supplementary information) gives such a compilation for the aluminides, Tables S2–S4, presented in the electronic

Table 1 Energies, Bader-charges und basin volumes of binary aluminides of earth alkaline elements

Compound AE mol fraction Structure type	*Space group* Calculated lattice parameters (Å) a/b/c α/β/γ	Atom type and Wyckoff site (according to cif)	Bader charges/basin-volumes (Å^3) individual and *mean* bonding numbers	Energy/Atom (eV) *formation enthalpy (meV)*
Mg	$P6_3/mmc$ 3.201/5.197	2c	0/23.05	-1.517
Ca	$Fm\bar{3}m$ 5.501	4a	0 /42.52	-1.900
Sr	$Fm\bar{3}m$ 6.005	4a	0/54.13	-1.650
Ba	$Im\bar{3}m$ 5.025	2a	0/63.44	-1.888
Al	$Fm\bar{3}m$ 4.042	4a	0/16.59	-3.748
Mg_xAl_y	Solid solutions of Mg and Al in hcp Mg- or fcc Cu-type structures and in cubic or hexagonal Laves phases			
$Mg_{17}Al_{12}$ 0.59 cI58 Mn-type	$I\bar{4}3m$ 10.544	Mg1 2a; Mg2 8c; Mg3 24g; Al 24g;	1.32/8.98 1.13/11.04 1.14/10.36 -1.63/34.06 3 *3*	-2.449 *-17*
$Mg_{13}Al_{14}$ 0.48 cI54 Sb_2Tl_7-type	$Im\bar{3}m$ 10.204	Mg1 2a; Mg2 24h; Al1 12e; Al2 16f;	1.46/7.01 0.81/12.78 -1.0/27.93 4 -0.66/25.45 4 *4*	-2.576 *101*
$Mg_{23}Al_{30}$ 0.43 hR159-type	$R\bar{3}H$ 12.719/21.924	Mg1 3b; Mg2 6c; Mg3 6c; Mg4 18f; Mg5 18f; Mg6 18f; Al1 18f; Al2 18f; Al3 18f; Al4 18f; Al5 18f;	0.91/13.22 1.33/8.42 1.38/8.34 1.33/8.71 1.29/8.95 1,30/8.93 -0.70/23.47 6 -0.85/25.83 5 -0.85/25.86 5 -1.01/27.03 4+1 -1.56/34.04 3 *4.8*	-2.788 *9*
$MgAl_2$-I 0.33 $HfGa_2$-type	$I4_1/amd$ 4.171/25.080	Mg 8c; Al1 8c; Al2 8c;	1.44/6.52 -0.35/28.46 6 -1.09/27.55 6 *6*	-2.999 *13*

Compound AE mol fraction Structure type	*Space group* Calculated lattice parameters (Å) a/b/c α/β/γ	Atom type and Wyckoff site (according to cif)	Bader charges/basin-volumes (Å^3) individual and *mean* bonding numbers	Energy/Atom (eV) *formation enthalpy (meV)*
$MgAl_2$-II 0.33 Hexagonal Laves phase	*$P6_3/mmc$* 5.477/8.748	Mg 4f; Al1 2a; Al2 6h;	1.47/8.59 -0.68/24.02 6 -0.69/24.15 6 *6*	-3.046 *-6*
Ca_8Al_3 0.73 Ca_8In_3-type	$P\bar{1}$ 9.510/9.585/9.673 98.93/101.09/119.63	Ca1 2i; Ca2 2i; Ca3 2i; Ca4 2i; Ca5 2i; Ca6 2i; Ca7 2i; Ca8 2i; Al1 1c; Al2 1f; Al3 2i; Al4 2i;	1.11/19.63 1.12/19.11 1.13/19.20 1.13/18.99 1.10/20.87 1.13/19.06 1.05/20.60 1.06/20.24 -3.08/69.6 0 -2.91/67.67 0 - 2.88/65.94 0 -2.94/67.16 0 *0*	-2.560 *-161*
$Ca_{13}Al_{14}$ 0.48 Fe_3Al-type analogue	*C2/m* 15.591/9.838/9.714 90/108.28/90	Ca1 8j; Ca2 8j; Ca3 4i; Ca4 4i; Ca5 2c; Al1 8j; Al2 4i; Al3 4i; Al4 4i; Al5 4h; Al6 4g;	1.21/16.50 1.19/16.434 1.20/17.20 1.23/15.77 1.11/18.44 -1.08/34.11 3 -1.27/36.69 2+1 -1.16/37.26 3 -1.12/37.97 3 -1.39/37.51 3 -0.69/28.33 4 *3.14*	-3.112 *-251*
$CaAl_2$ 0.33 Cubic Laves phase	$Fd\bar{3}m$ 8.054	Ca 8b; Al 16c;	1.19/15.00 -0.60/25.15 6 *6*	-3.480 *-342*
$CaAl_4$-LT 0.20 $CaAl_4$-type	*C2/m* 6.160/6.138/6.382 90/118.01/90	Ca 2a; Al1 4h; Al2 4i;	1.28/15.44 -0.01/20.65 4 -0.63/24.79 5 *4.5*	-3.568 *-190*
$CaAl_4$-HT 0.20 $BaAl_4$-type ($ThCr_2Si_2$-type)	*I4/mmm* 4.381/11.172	Ca 2a; Al1 4d; Al2 4e;	1.29/15.55 -0.06/21.11 4 -0.59/24.73 5 *4.5*	-3.573 *-195*

supplementary information, contain this information for the other trielide compounds.

All compounds presented here are known to exist. They have been prepared and their structures have been determined by X-ray crystallography. There have been erroneous assignments of structure types in some cases based on poor X-ray data which were corrected by other authors (e.g., Sr_3Al_2/Sr_8Al_7, $SrAl/Sr_8Al_7$[16] or $Ba_7Al_{13}/Ba_{21}/Al_{40}$[29]). All DFT calculations started

Compound AE mol fraction Structure type	*Space group* Calculated lattice parameters (Å) a/b/c α/β/γ	Atom type and Wyckoff site (according to cif)	Bader charges/basin-volumes (Å^3) individual and *mean* bonding numbers	Energy/Atom (eV) *formation enthalpy (meV)*
Sr_2Al 0.67 mC24-type	*C2/c* 14.780/9.749/7.515 90/119.23/90	Sr1 8f; Sr2 8f; Al 8f;	1.09/27.80 0.89/30.8 -1.99/57.85 0 *0*	-2.350 *0.008*
Sr_8Al_7 0.53 Sr_8Al_7-type	*P2$_1$3* 12.763	Sr1 4a; Sr2 4a; Sr3 12b; Sr4 12b; Al1 4a; Al2 12b; Al3 12b;	1.18/24.94 1.19/25.92 1.14/26.70 1.14/27.64 -1.26/41.15 3 -1.22/41.84 3 -1.43/46.40 2 *2.57*	-2.809 *-168*
Sr_5Al_9 0.36 Sr_5Al_9-type	$R\bar{3}m$ 5.882/35.62	Sr1 6c; Sr2 6c; Sr3 3b; Al1 18h; Al2 6c; Al3 3a;	1.15/21.71 1.14/20.08 1.23/24.23 -0.58/25.60 3+1 -1.00/34.77 3 -0.49/24.65 6 *4*	-3.260 *-267*
$SrAl_2$-I 0.33 Cubic Laves phase	$R\bar{3}m$ 8.280	Sr 8b; Al 16c;	1.13/20.33 -0.56/25.31 6 *6*	-3.302 *-246*
$SrAl_2$-II 0.33 $CeCu_2$.type	*Imma* 7.895/4.842/7.900	Sr 4e; Al 8h;	1.19/21.01 -0.59/27.25 4 *4*	-3.305 *-249*
$SrAl_4$ 0.2 $BaAl_4$-type	*I4/mmm* 4.471/11.198	Sr 2a; Al1 4d; Al2 4e;	1.26/20.44 -0.08/21.43 4 -0.55/24.30 5 *4.5*	-3.556 *-228*
Ba_4Al_5 0.44 Ba_4Al_5-type	*P6$_3$/mmc* 6.086/18.193	Ba1 4f; Ba2 4e; Al1 4f; Al2 6h;	0.82/36.74 0.79/36.19 -0.96/36.90 3 -0.48/25.50 4 *3.6*	-3.150 *-220*
Ba_7Al_{10} 0.41 Ba_7Al_{10}-type	$R\bar{3}m$ 6.067/49.52	Ba1 6c; Ba2 6c; Ba3 3b; Ba4 6c; Al1 6c; Al2 6c; Al3 18h;	0.94/30.11 0.79/34.43 1.17/33.18 0.88/36.13 -0.99/36.33 3 -0.82/33.26 3 -0.45/25.50 4 *3.6*	-3.221 -239
Ba_3Al_5 0.38 Ba_3Al_5-type	*P6$_3$/mmc* 6.066/14.618	Ba1 4f; Ba2 2a; Al1 4f; Al2 6h;	0.93/29.88 1.07/33.96 -0.85/33.22 4 -0.41/25.50 3 *3.4*	-3.294 *-256*

from literature data given in the data bases. One way to determine whether a structure given is correct could be a validation of the calculated energies in comparison with other structure proposals. However, this cannot exclude that a compound with such a structure exists under special synthesis conditions even though the energetics would argue against it.

From DFT calculations we may estimate the formation enthalpies of A_xB_y compounds (H^{AB}) according to $H^{AB} = E^{AB} - x\,\mu_A - y\,\mu_B$, where E^{AB} is the total energy of the compound per formula unit as calculated by DFT and μ_A and μ_B are the chemical potentials of the elements A and B which are generally equivalent to the DFT ground state energies of the elements in certain standard conditions. (There are special cases where there is a need for additional corrections.)

It is customary to discuss the stability of compounds by plotting so-called hull curves where the energies per atom resulting from the DFT calculations – also given in Table 1 (and in Tables S1 to S4) – are compared for different compounds in varying stoichiometric relations. (For examples see [18]). We speak of a convex hull system when the hull-profile descends below the line joining the energies of the end members in a series of related compounds. The degree to which this happens is the energy gain on compound formation from the constituent atoms, i.e., the formation enthalpy defined above. We have included these formation enthalpies per atom (f.e./atom) in the graphs showing such hull curves (Figure 2a–d) for the aluminides as an example. The convex hull is found for phases that have an energy lower than any other phase or linear combination of phases with different amounts of the same elements resulting in the same overall composition. However, it must be kept in mind that DFT calculations describe a T = 0 [K], P = 0 [bar] state. Energy relations may be different when the volume term ($p\Delta V$) and the entropy term ($T\Delta S$) adds up to the total free energy of the system. Nevertheless, an analysis of such curves may help to understand phase diagrams of such binary systems.

As a first example we show the hull curve of the Mg–Al system which is an extreme one for such a discussion (Figure 2 a). As said before, we have omitted alloys whith a compositional range or examples with partial occupancy of sites and statistical distribution of different atoms in our compilation which abound in the Mg–Al system. The few compounds listed here are assumed to exist as line phases. Of them only the second variant of $MgAl_2$ and $Mg_{17}Al_{12}$ meet the condition of being a convex member. It is interesting to compare this finding with the Mg–Al phase diagram[19] where there is only one faint trace of a distectic compound around the 1 : 1 ratio with a broad range of composition. A peritectic point can be located at about 0.42 mol fraction of Mg which is probably the representative of $Mg_{23}Al_{30}$. Besides these two there are only solid solutions of the elements at the borders of the diagram. $MgAl_2$ itself does not stand out in this phase diagram. The hull curve clearly shows that entropic effects have certainly played a major role in the synthesis of these compounds. They will not exist at T = 0 [K]/ P = 0 [bar] conditions.

The Ca–Al phase diagram[20] shows a prominent dystectic point at a mol fraction of 0.33 ($CaAl_2$). Ca_8Al_3 is weakly distectic and the compounds $CaAl_4$ and $Ca_{13}Al_{14}$ decompose peritectically. This is nicely reflected in the hull curve (Figure 2b) where only $CaAl_2$ is clearly convex in relation to the neighbouring compounds and Ca_8Al_3 is a borderline example lying on the line joining $Ca_{13}Al_{14}$ and Ca.

A similar situation is found for the Sr–Al system[21] where only $SrAl_4$ is known to melt dystectically whereas $SrAl_2$ and Sr_8Al_7 decompose peritectically. There is no indication for the existence of Sr_5Al_9 in the phase diagram though its position on the hull curve is slightly convex in relation to the neighbouring compounds (Figure 2c).

Finally, the hull curve of the Ba -Al system (Figure 2d) indicates that only $BaAl_4$ and Ba_4Al_5 are clearly stable against decomposition, whereas $Ba_{21}Al_{40}$ again represents a borderline situation. (The latter compound has erroneously been described as Ba_7Al_{13} in early publications.) And, indeed, we find only these compounds in the phase diagram.[22] $BaAl_2$ is known only in a high-pressure form as cubic Laves phase and should not be stable under normal conditions according to the hull curve.

We have assembled such hull curves for all the other alkaline earth-trielides in the supplementary information (Figure S1 in ESI). Looking at them in their entirety we see similar types as the ones presented for the aluminides. All Mg-TR hull curves look alike excepting perhaps the one for the Mg–Ga system where all compounds lie slightly below the line connecting the elements. As mentioned before Mg rather tends to form non-stoichiometric alloys, and the "line" phases described in literature are probably serendipity choices of almost stoichiometric samples and their structure determinations are hampered by the extremely weak X-ray contrast of the electron density of Mg and Al. The hull curve of the Ba–Ga system resembles that of the Sr–Al type with one of the phases in a concave situation. The indides of Sr and Ca and the thallides of Ba show hull curves like the Ba–Al system with some members not convex in relation to neighbouring compounds. All the other hull curves resemble the one shown for the Ca–Al system.

To summarize this paragraph, we may state that there is a general trend in the hull curves giving the formation enthalpies of binary AE-trielide compounds. The convex nature, i.e., the distance of the individual compounds from the line connecting the two elements, increases when going down the AE group from Mg to Ba. The difference between the energy of an element mixture without chemical reaction and of the possible compounds formed on reaction, i.e., the formation enthalpy, is negligible or small for Mg compounds, and it increases on going down the AE group. Formation enthalpies per atom (given in eV in the graphs) range up to about −0.3 for aluminides, −0,45 for gallides and indides and −0,4 for thallides (see the corresponding figures in ESI). So, the electropositive nature of the alkaline earth is very important and the polarity, i.e., the electrostatic contribution to the overall lattice energy plays a decisive role for the stability of these compounds (see below). Looking at the typical paraboloid-like form of these hull curves we recognise that the formation enthalpies are highest in lower to medium AE mol fractions where a "composition weighted electronegativity difference" ($\Delta EN \cdot y/x$ for AE_xTR_y, as

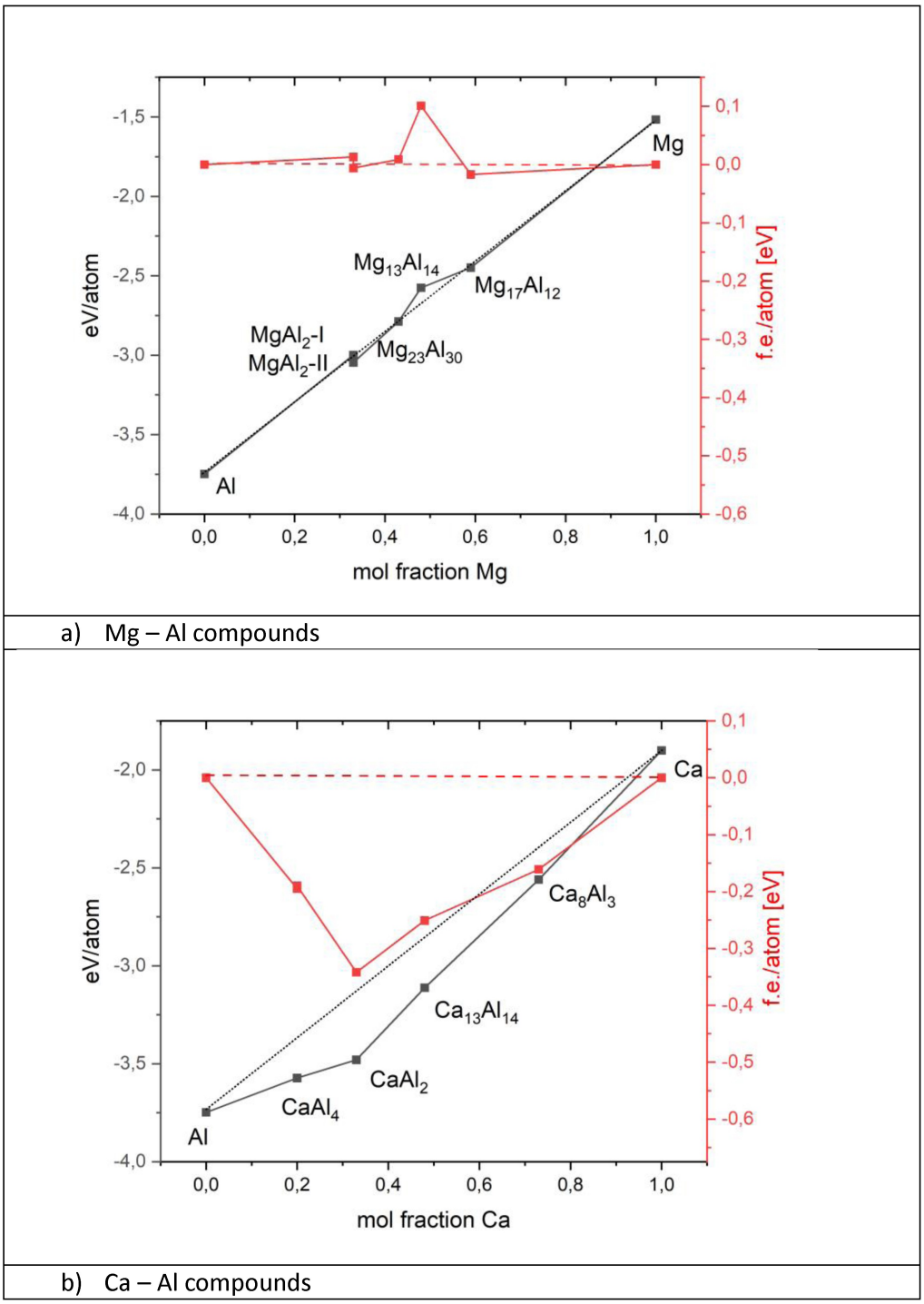

Figure 2. Hull curves of Aluminides.

used also in the PCA calculations, see below) has its maximum influence. They generally decrease on approaching the borders of the composition ranges where one or the other partner predominates.

A detailed study of such hull curves in comparison could help to create new ideas with respect to synthesis strategies and to find new compounds with other compositions of these elements or polymorphic transitions under varying temperatures and pressures. Compositions and matching structures found for other element combinations could be used as starting points for DFT relaxation calculations. Depending on the calculated energies and the position within such hull curves one could devise synthesis strategies to get hitherto unknown compounds by varying the conditions of synthesis in P and T

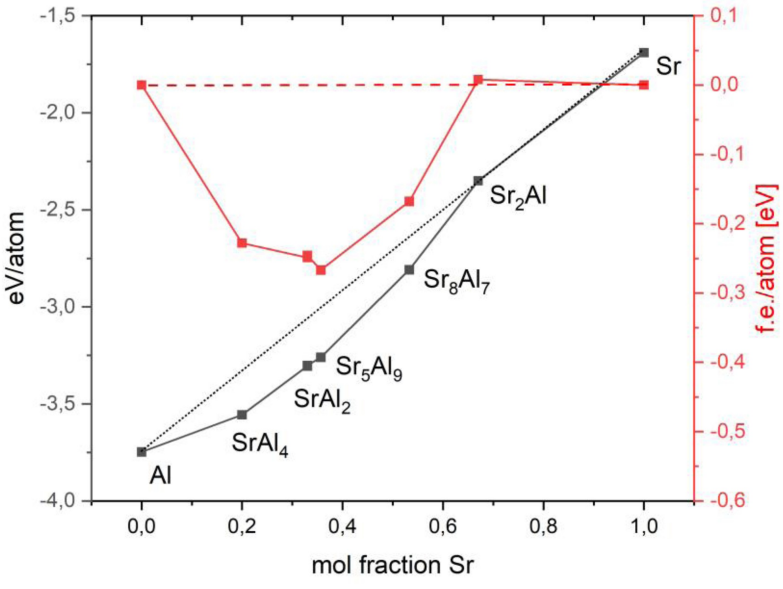

c) Sr – Al compounds

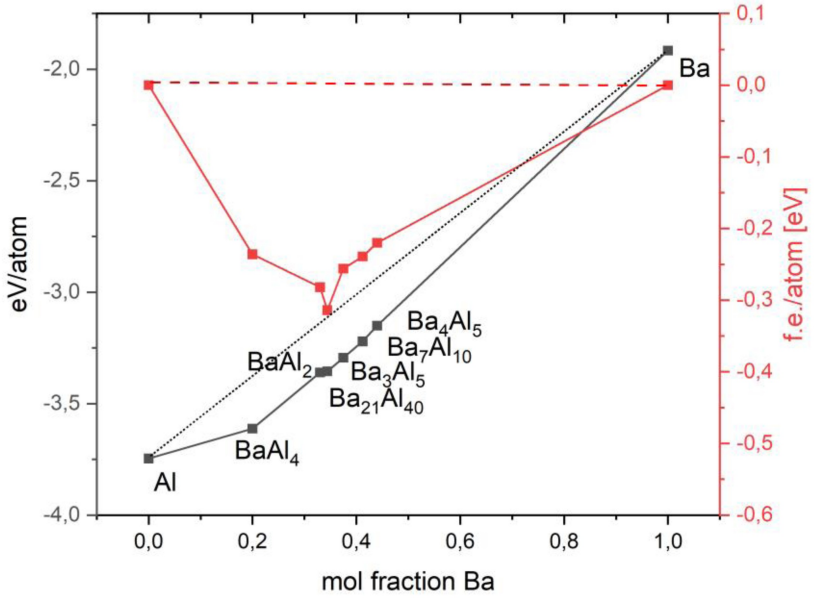

d) Ba – Al compounds

and by enhancing entropic effects via mixing of different elements.

The Development of Charges and Bonds in AE_xTR_y-Compounds

In a formal approach we may express the Zintl concept for simple binaries A_xB_y by the formula $b = 8-(N+n\cdot x/y)$, where b is the number of bonds expected between the B element atoms, N is its main group number while n is the main group number of the A element. We "assume" an electron transfer from the more electropositive element to the other one which "creates" a ψ-element to the right in the PSE for the B atom and thereby adopts its bonding characteristics.

An inspection of the number of bonds between the trielide atoms in the Tables (Table 1 and S1, Tables S2 to S4) reveals some interesting aspects. As said above, we do not expect to

see any bonds at AE contents above 0.7 according to the Zintl principle, and for compositions with lower AE content we could "imagine" specific bond numbers or even mixtures of several bond numbers to comply on the average with the Zintl counting rule given above. Indeed, we find no examples with TR-TR-bonds beyond the said AE-content. However, there are many cases where our counting rules do not really hold to understand the pattern of bonding in these compounds. In Figure 3 we plot the bond numbers found in these binary AE-trielides together with the "expected" ones according to the Zintl-formula given above which may be transformed to b = 5−(2·mF/(1-mF) to have the mol fraction (mF) as direct parameter.

There is considerable scatter away from our expectations especially for lower mol fractions of AE atoms. The compounds marked separately are mostly Mg aluminides and some indides having typical alloy structures like CuAu or CsCl and others where the trielide atoms cluster in sheets or columns giving high bond numbers. *Examples fully complying with the Zintl counting rules are rather rare.*

One "good" example could be seen in the $BaAl_4$-type structures (see below) where the formal transfer of 2 electrons from Ba to the 4 Al atoms (i.e., $^1/_2$ per Al) could form 2 ψ-Si with 4 bonds and leave 2 Al with their own valence electron number needing 5 bonds to attain a noble gas element configuration, and this is indeed the bond pattern of these compounds. A mixture of several bond numbers can meet the required number on the average. Another "electron precise" example is found in the rather complicated structure of Ba_7Al_{10}. We could imagine a formal transfer of 14 valence electrons from Ba to 10 Al atoms giving 4 of them as ψ-P and 6 further ones as ψ-Si both with the bond number of these elements, and this is just as we see it in this structure. Other hits for such counting rules would be compounds with a KHg_2- (or $CeCu_2$−) type structure such as $BaIn_2$ or the orthorhombic modification of $SrAl_2$. But, as said before, these are rare examples. In most cases the formation of bonds cannot be described by such considerations. If they were, we could perhaps have expected semiconducting behaviour, however, all compounds described here are metallic and show either no gap at all or pseudo gaps in the DOS diagrams at the Fermi level. We have abstained from including DOS diagrams in this paper since many of them have been shown in detail by others.[17,23,24] It is widespread opinion that d-orbitals of the alkaline earth atoms can contribute to the states near E_F forming a broad conduction band in this region.

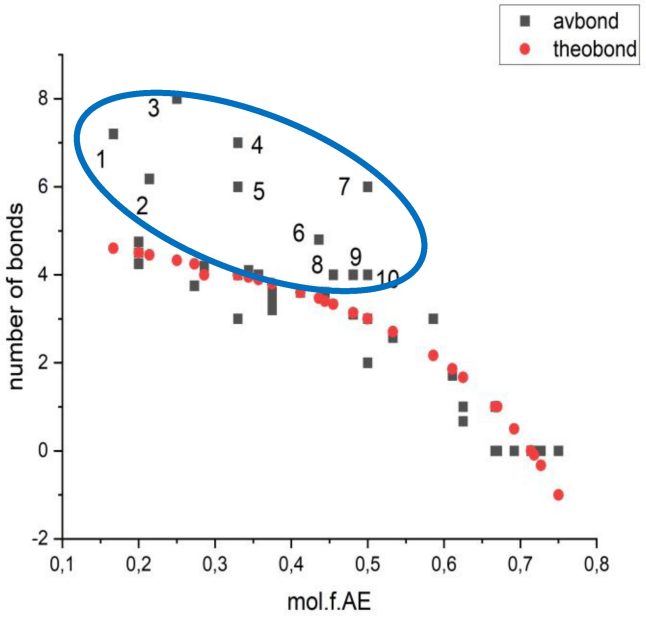

Figure 3. Formal average bond numbers (given in red spheres) and real ones (black squares) found in the group of binary alkaline earth trielides vs. AE mol fraction, marked compounds: 1 $SrIn_5$ 2 Sr_3In_{11} 3 $SrIn_3$ 4 $MgAl_2$-l 5 $MgIn_2$ 6 $Mg_{23}Al_{30}$ 7 CaIn–l 8 Ba_5Ga_6 9 $Mg_{13}Al_{14}$ 10 MgIn.

We take Ba_3Al_5 as another example where 6 electrons could be transferred giving 1.2 electrons per Al, i.e., 4 of them taking up one and 1 taking up two, and we expect 4 Al with 4 bonds and 1 with 3 bonds. However, the real structure shows two fourfold-bonded Al and three Al with three bonds. Such a bonding scheme would need a transfer of 8 electrons according to the Zintl concept instead of the expected 6 electrons. For Ba_4Al_5 Zintl-counting would forecast 3 threefold bonded and 2 doubly bonded Al atoms. In this structure we find twice three bonds and three times four bonds, i.e., an "electron transfer" of 7 instead of 8 electrons. So, the simple idea of electron transfer according to the AE content must be put into question.

A closer inspection of such data in the tables (Table 1–4) together with the listed Bader charges may be helpful. We have also quoted arithmetic mean bond numbers for all compounds, and in the following plot (Figure 4) we compare their variation with growing content of the AE component with the development of the trielide charges and we also show the difference between them and the "formally transferable" electrons taking Ca–Ga compounds as an example.

Corresponding plots for other AE-TR systems have virtually the same appearance. As expected, we see an increasing average negative charge on the Ga atoms with increasing Ca content. The number of bonds decreases with growing "transfer pressure" according to the Zintl concept, however, there is not a steady change, the individual topologies make their mark, and in other element combinations such curves are even more rugged. The third, rising curve gives the deviation from the formally possible electron transfer and the real one, and this transfer is evidently slowed down more and more with increasing AE content. So, there is a first bias for our prediction of the bonding scheme.

Looking at the individual charges for the different structures in our tables we notice that they vary for different Wyckoff sites. The average charges of the cationic species decrease slightly with rising AE content, there are more and more of them in relation to the TR atoms, and each one of them will contribute less and less since the possible "uptake" by the trielide sublattice is finite. The individual charges for different Wyckoff sites for A atoms do not vary much. The one and only exception would be the Ca atom on the 4b site in $Ca_{11}Ga_7$ with a Bader charge of 0.36 in comparison to three other ones with charges

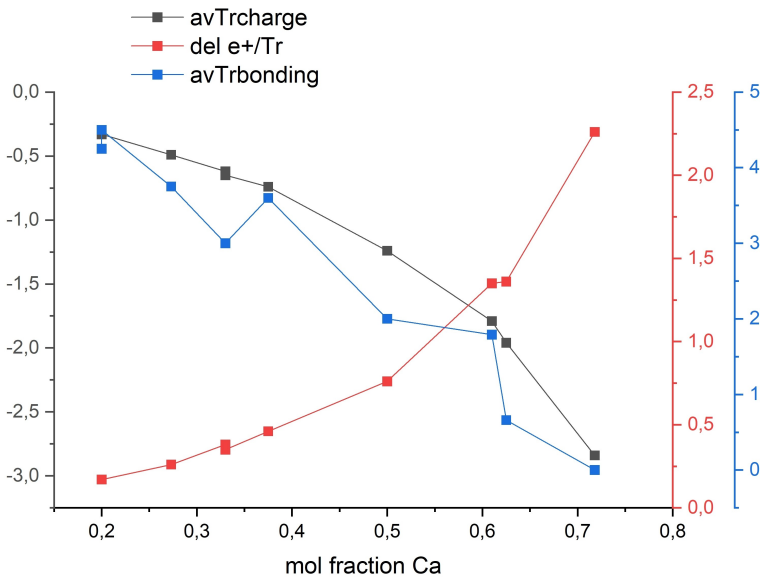

Figure 4. Plot showing the variation of mean bond numbers (avTrbonding) with increasing Ca-content in binary Ca–Ga compounds together with the Bader charges (avTrcharge) for Ga and the difference between the total number of valence electrons and the "real transfer" (del e+Tr) as noted in the Bader charges of Ga.

around 1.1 to 1.2. This may be explained by a topological analysis (see also next paragraph). In Figure 5 we see this atom surrounded by other Ca atoms in a 12-fold coordination in the centre of a cuboctahedron. Within its "metal-like" surrounding there is no contact with Ga atoms, whereas the other Ca atoms all have Ga neighbours setting up some local polarity. For the isotypic $Sr_{11}In_7$ we find the same charge distribution among the different Sr sites.

The charges of the anionic partners differ considerably depending on the number of bonds each atom is engaged in. The correlation between negative charge of the TR atoms and bond numbers is striking. The charges drop with an increasing number of bonds between the trielide atoms, i.e., the formation of bonds reduces the electron transfer from the electropositive partner driven first by the electronegativity difference ΔEN. This difference in "effective ΔEN" depending on the number of bond contacts is clearly visible in individual atoms in the structure. So, *a "stronger bonded" ensemble of trielides is a seemingly less electronegative partner in the system*, or, giving it in a different approach, *there is a sort of "mechanism of buffering*

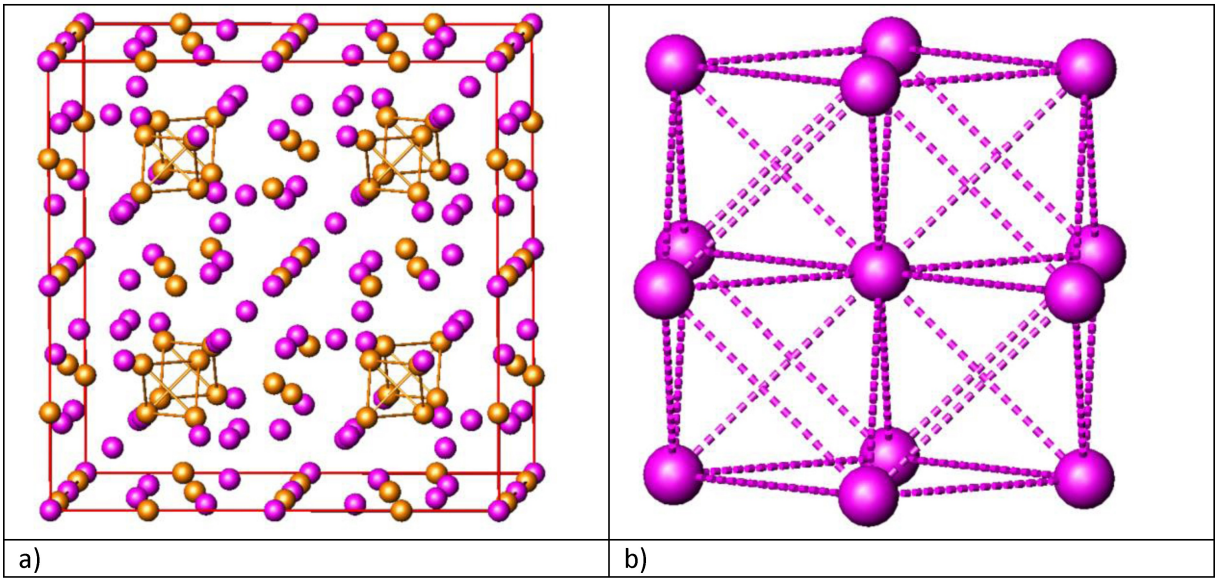

Figure 5. The structure of $Ca_{11}Ga_7$, a) complete unit cell b) local distribution of Ca atoms around the Wyckoff site 4b [0.5 0.5 0.5] at the centre of the cell.

by bonding" working against an electron transfer as initially imposed by ΔEN. Bonding in the anionic lattice reduces the pressure for such an electron transfer, thereby reducing the polarity in the system which goes together with a decrease of Madelung-type contributions to the lattice energy. Keeping in mind that their weight in the balance sheet of the total lattice energy is very large, we may wonder how bonding compensates for that. But this is just the challenge to our understanding to accept how the mutual optimization of the Madelung energy and space filling can override the usually dominating factor of electron count and bonding.[25] It has not yet been possible to quantify the interplay of all these factors determining the structural topology and the stability of these phases.[23] (A small excursion into a more detailed discussion is given in the next section.)

It has frequently been argued that there may be delocalized bonding in such compounds which may reduce the individual charges for the atoms,[33] chemists and physicists have developed quite different views on this topic. There is even some debate trying to distinguish between electron-poor and electron-rich multicentre bonding in these phases. There may be no need to distinguish such classifications when joining the physicists view on mixing of several bands to form more or less broad conduction bands which are then partly filled.

However, keeping in mind that DFT calculations give an electron density in real space, we must state that the electron numbers integrated within various basins also include electrons in bond regions such as in so-called critical points which can be located by appropriate programme codes[26,27] or by plotting ELF functions. So, even including this electron density the overall electron transfer is considerably reduced in systems with TR-TR bonds!

The Role of Madelung-Type Contributions to the Overall Energy of AE_xTR_y Compounds

It is common practice to dig out Born-Haber cycles when discussing the different contributions to the overall energy of crystalline compounds. In doing so we sum up energies to spend or to gain in various hypothetical steps of the formation of such a compound starting from the elements. We add up the energy necessary to bring the elements into the gaseous state and to atomize and ionize them to the desired oxidation state. By the formation of anions, we may gain energy in some cases. However, the cost function up to this step, will always be negative. In the last step in a simple Born-Haber cycle the energy gained in the crystallization process usually balances any expenses before, and of this energy the electrostatic contribution is by far the most important part especially when ionicity brought about by high ΔEN values is a major aspect of bonding in a compound. Other contributions such as bond formation and London dispersion interactions will then play a secondary role. For different structures of the same compound the cost function for the first steps of such a cycle will be the same, the difference between the final energies will arise from the different contributions pertaining to bond energy and electrostatic energy.

As said before, Bader analyses of the compounds discussed here show varying charges, and calculations of the Madelung Part of Lattice Energy (MAPLE) may help to estimate their portion in the total balance of the cost function. (We must keep in mind that the total formation enthalpy (f.e.) which we may thereby calculate in such a cycle is not to be compared with experimental formation energies given in the JANAF tables since the entropy part for the total free energy is missing.) As an example, we compare MAPLE values of several di-trielides with the corresponding energy per atom in Table 5 and present them as a graph in Figure 6. (The numbering in the graph follows the list in the table.)

Table 5 MAPLE and total energies, cation charges and bond numbers for AE-ditrelides

Compound Structure type	MAPLE/atom (eV) COUPOT	Energy/atom (eV) VASP	f.e. (meV)	Δ (eV)	av AE charge	av TR charge	av bond number
$CaAl_2$ cub Laves	-2.201	-3.480	-342	-1.275	1.19	-0.60	6
$SrAl_2$-I cub. Laves	-1,912	-3.302	-246	-1.390	1.13	-0.56	6
$SrAl_2$-II $CeCu_2$	-1.984	-3.305	-249	-1.321	1.19	-0.59	4
$BaAl_2$ cub Laves	-1.218	-3.360	-282	-2.142	0.91	-0.46	6
$CaGa_2$-I AlB_2	-2.958	-3.036	-445	-0.348	1.30	-0.65	3
CaGa-II $CaIn_2$	-2.879	-3.037	-479	-0.158-	1.23	-0.62	4
$SrGa_2$ AlB_2	-2.746	-2.961	-452	-0.215	1.31	-0.65	3
$BaGa_2$ AlB_2	-1.982	-3.023	-436	-1.041	1.16	-0.58	3
$CaIn_2$ $CaIn_2$	-2.720	-2.763	-410	-0.043	1.25	-0.62	4
$SrIn_2$ $CaIn_2$	-2.600	-2.715	-445	-0.115	1.24	-0.62	4
$BaIn_2$ $CeCu_2$	-1.832	-2.828	-479	-0.996	1.10	-0.55	4
$SrTl_2$ $CaIn_2$	-2.684	-2.374	-330	0.310	1.27	-0.64	4
$BaTl_2$ $CaIn_2$	-2.187	-2.517	-395	-0.330	1.14	-0.57	4

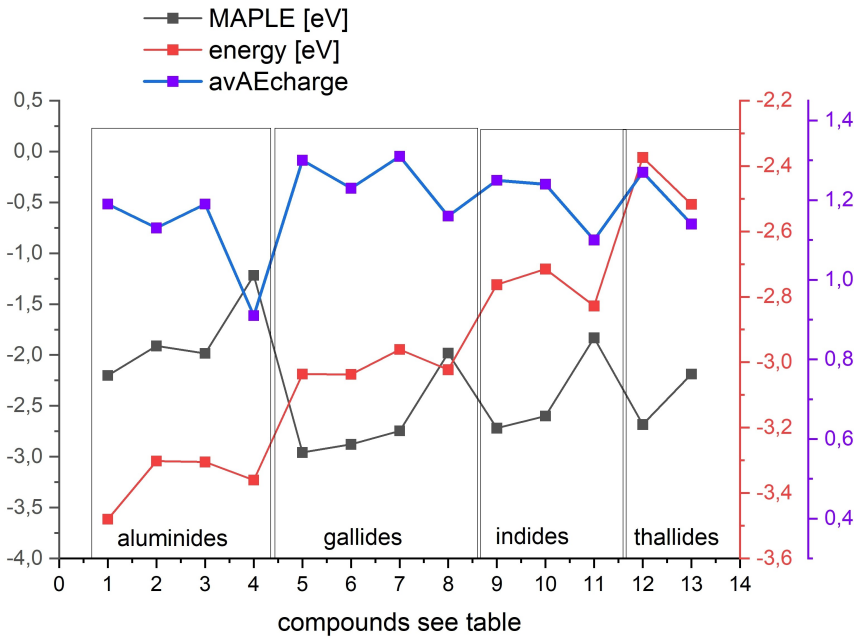

Figure 6. Madelung Part of Lattice Energy (MAPLE, COUPOT[5]), energy per atom (VASP) and cation charge (numbering as in Table 5).

The lines connecting the AE-charges and the overall energy have very similar trends, and this shows that the ionic contribution to the total energy is formative. In each group of AE-trielides the charges decrease from the Ca to the Ba compound and the dilation of the structures due to the growing size of the AE component reinforces this effect on the MAPLE values. This variation of charges is then also reflected in the trend of the energies. Nevertheless, the difference between both energies is largest for the Ba compounds in each series though the electrostatic part is reduced. The overall energy is largest for just these Ba compounds in comparison to the neighbouring ones. This is a seemingly paradox finding since we may expect a growing ionicity in the respective series when recurring to ΔEN values only which should increase the lattice energy and the overall stability of the respective compounds. We see another mechanism effective in the balance of the cost function, namely the "individuality of interacting elements". *Electron transfer and its effect on the bonding situation is not only governed by "ΔEN-pressure" but*, to use a more atomistic picture, also *by the compatibility of electronic states in the atoms with respect to their energies and the associated spatial allocation*. In a more collectivistic language, we may speak of energy gaps in the band structure between bands with high local character, and this difference is largest for the pair Ba–Al. The "misfit" is reduced in the line of the pairs Ba–Ga, Ba–In and Ba–Tl. The ΔEN-paradox is thereby cancelled!

To compensate for the loss of electrostatics the energy set free by bond formation plays an increasing role in the total balance of the cost function and it will depend on the bond numbers and/or the type of bonding. By comparison of these parameters for the different structures we may conjecture that multicentre-type bonding plays a larger role especially in some cases with high bond numbers, whereas two-centre-type bonding will be the prevailing interaction for the compounds in this list with three- and fourfold bonding. Both types will contribute differently to the term "bond energy" in the total cost function of these systems.

An Analysis of the Topology of Bonds in View of Varying Bader Charges

In Figure 4 we have focussed on average bond numbers for a first analysis of bonding and in the discussion given above we have demonstrated that the variations of charges and bond numbers may be considerable within one compound, and this, in turn, determines the topology of the structures. There is once again the question about the primacy of causes, the hen or egg conflict. First, is the distribution of charges a result of a specific structural arrangement determined by other factors (see also chapter on PCA), or does a need to balance charges in a specific way by means of bond formation lead to a particular topology? And second, can we retrace the individual charge and bond pattern in a structure from an analysis of the structural arrangement? In other words, can we "understand" the differences among the TR charges for different Wyckoff sites?

As a first example we study the variation of the Ga charges in the (*I4/mmm*) form of $CaGa_4$ ($BaAl_4$-type), see Figure 7). There have been very detailed studies of the bonding in this structure type.[28a,b] A simpler picture may also help to understand the distribution of charges. There are two different Ga atoms in Wyckoff positions 4d and 4e with 4 and 5 bonds to neighbouring Ga atoms and a Bader charge of −0.21 and −0.44 respectively.

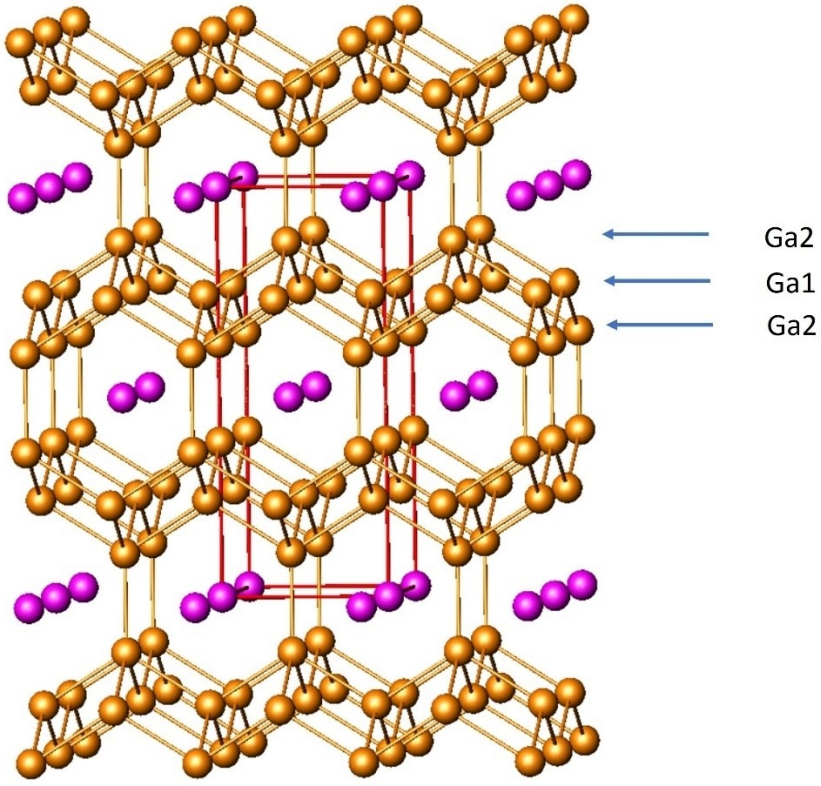

Figure 7. The structure of $CaGa_4$ ($BaAl_4$-type) in a view approximately along [100], the different crystallographic sites in a triple layer are marked.

We may describe the partial Ga structure as made up of triple layers – resulting from square nets of Ga atoms (Ga1 Wyckoff set 4d) which are capped alternately above and below the plane by apical Ga atoms (Ga2 Wyckoff set 4e) – with a layer of Ca cations separating them. Ga1 atoms, exerting 4 bonds, make up the middle layer and Ga2 atoms are in the outer layers. Depending on the distance to the next triple layer they form a fifth bond in the various compounds which crystallize in this structure. Looking at the number of bonds only we might expect the Ga2 atoms to have the lower charge. The "unexpected" difference between the Bader charges may be understood seeing Ga1 (Wyckoff site 4d) in a purely "quasi-metallic" environment and Ga2 (Wyckoff site 4e) exposed to the influence of the neighbouring Ca cations which enhances the polarity and thereby their charge. So, the specific electron transfer takes effect on the bond topology of the structure and this in turn influences the individual charges. (By the way, this difference between the two sites also explains the localization of Cr and Si in the ternary variant of this structure type ($ThCr_2Si_2$-type) where the less electronegative element Cr prefers the 4d site.) This thinking focusses on the local electron distribution in real space whereas in band structure calculations we would "try" to find such localizations in the weight of specific atomic orbital sets in the "character" of certain bands.

We may depict this principle in more detail. For the aluminides we find this structure type with Ca, Sr, Ba as the AE component. It is interesting to note that the charges for these two types of trielide atoms vary differently with increasing ΔEN. Looking at the 4d and 4e site in the series $CaAl_4$–$SrAl_4$–$BaAl_4$ we find the combinations −0.06/−0.59, −0.08/−0.55, −0.13/−0.41 respectively in this row of compounds. The charge on the 4d site follows the ΔEN sequence a little, that one on the 4e site decreases noticeably with growing electronegativity difference. First, the fifth bond of these atoms strongly counteracts the influence of EN. Second, we have pinpointed the effect of polarity developing in the neighbourhood of cations as the cause for higher charges on the 4e site, and this effect is slowed down in the given series by larger distances due to the increasing size of the cations. So, there is a fine interplay between electronic and topological issues. We will discuss further "conflicts with our expectations" below when dealing with Laves phases.

As a second example we choose the structure of $Mg_{13}Al_{14}$ ($Im\bar{3}m$) given in Figure 8 where there are also two different sites for four-bonded Al atoms, Al2 with three shorter (2.13 Å) and one longer bond (2.85 Å) and Al1 with four such longer bonds. Though the number of bonds is formally the same the difference in charges (−0.66 and −1.0, respectively) can now clearly be attributed to the difference of bond length. Therefore, not only the number but the "quality" of the bonds also plays a role in this game. *The amount of electron transfer* – and consequently the charge of the atoms – *varies with the length of*

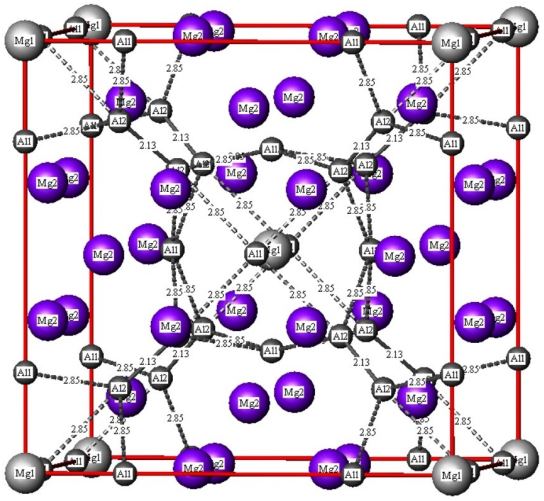

Figure 8. The structure of $Mg_{13}Al_{14}$ in a view approximately along [100]. Longer bonds are dashed.

the bonds, or – giving it in a different picture – *the electron transfer "mediates" the distance between the bonded partners*!

So, overall, we may summarize that the variation of the charges can be rationalized in comparison with the respective number of bonds and their lengths which can be seen as a representative of bond strength. The formation of shorter/stronger bonds reduces the electron transfer from the more electropositive partners. Furthermore, the charges of the anions will be influenced by the number and charge of cations in the close neighbourhood. Such findings may strengthen our belief in the significance of Bader charges as a means to rationalize structural details. They even help to decide whether there is a bond or not when distances alone will not help. However, admittedly, there are cases where the relations of different Bader charges for individual sites are difficult to interpret based alone on bond number and bond length, especially when the variation of Bader charges is small.

On Volumes and Charges – Laves Phases as Outlaws in a Community

For solid compounds the overall lattice energy is decisive for their existence and relative chemical stability, and the volume of the unit cell, i.e., the volume per formula unit, is a main parameter for the energy optimization in DFT runs.

We may believe that such volumes result as the sum of the volumes of the constituent parts, but we know that these volumes vary depending on the type of chemical interaction. Atomic volumes depend on the environment they are embedded in. Volumes of ions depend on their coordination numbers, and they are different for oxides or sulphides, as an example, and atomic volumes in metals differ from those in covalent systems. So, looking up tables of radii will sometimes not help to understand structural details.

Another parameter given in our tables is the volume of the basins of the different atoms in various Wyckoff positions as calculated by Bader analysis which add up to the total unit cell volume. We clearly see the "effective sizes" of the different AE elements when comparing their corresponding values, and – to a smaller degree – we also see differences for different Wyckoff sites. The same holds for the trielide atoms, however, their volumes are severely affected by their bonding status as well and this goes along with the differences in charge as described above. As said before, these volumes "shrink" with the number of bonds they are engaged in. So, the joint impact of the triple "charge – bonding – volume" is documented in a consistent picture in all such structures of intermetallic compounds.

When looking at the volumes per atom (V/at) – without considering differences between cations or anions – we see a general trend in the AE-TR systems discussed in this paper. They increase as expected with the number of the larger AE atoms which enlarge the total cell volume. However, Mg compounds differ from the other AE-trielides. Their volumes slightly increase for aluminides, but they decrease in the rows of gallides, indides and thallides (not shown here) since Mg is smaller than these trielide atoms. Figure 9 shows the development of volumes per atom in binary aluminides as an example.

We find slight kinks in these curves at mol fraction 0.33. The cubic ($Fd\bar{3}m$) and hexagonal ($P6_3/mmc$) Laves phases fall outside the usual parameters in this group as they also do so in many other plots, e.g., in plots of the mean charge with varying AE mol fraction and of the relation between Bader charges and the formally possible electron transfer which are both lower than expected for such phases. These structures have often been described in textbooks as a very dense packing of atoms with specific size relations of the constituent atoms, and they have been correlated with certain valence electron concentrations (VEC) as well. VECs of these aluminides formally fit the picture but – excepting $MgAl_2$ – radius ratios don't. The growing electropositivity from Mg to Ba is not reflected in the Al basins which are all almost equal in size around 25.1 $Å^3$. *In view of the "charge – bonding – volume" triple the Laves phases constitute outliers in many aspects.* The volume per atom as well as the anionic charge is lowered compared to the other compounds in the rows. The "effective AE content" – or the "effective ΔEN" – seems lower than the stoichiometric composition, the electron transfer to Al is partially "blocked" by very high bond numbers which are well out of the range of any Zintl counting. Furthermore, it is surprising to see that, other than expected from ΔEN values, the Bader charges for Al decrease for the cubic Laves phases when going from $CaAl_2$ to $SrAl_2$ and $BaAl_2$. This goes in line with our observations for the $BaAl_4$-type compounds discussed above where effects of different electronegativity are counteracted by bond formation. Here too, the "induced local polarity" is reduced with the growing distances between the cationic species and the trielide sublattice in this series and this is the cause for the decreasing charges.

The tendency to form Laves phases is distinctly larger for aluminides than for gallides or indides. However, the size mismatch can be considerable. So, other solutions come into view. The formation of compounds with a composition close to

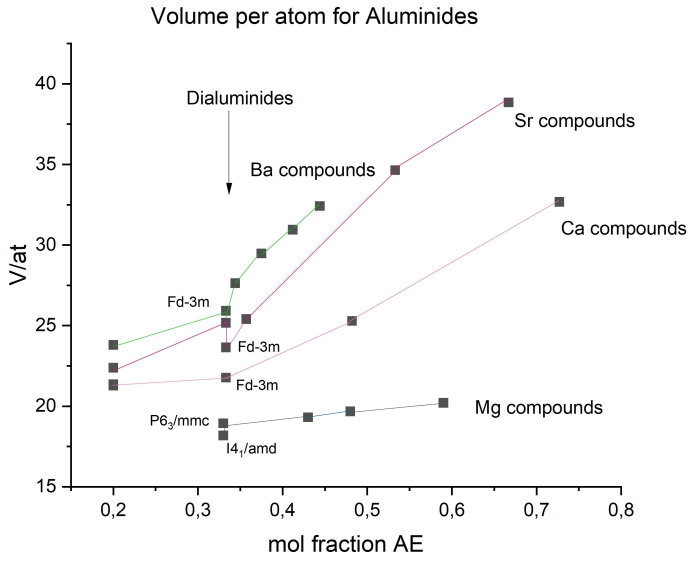

Figure 9. Volumes per atom (Å^3) in binary AE-aluminides vs. mol fraction of AE.

$AETR_2$, such as Sr_5Al_9 or Ba_7Al_{13} becomes important as stable alternatives which may be considered "as AE excess derivatives of Laves phases where the Al 3D network of the Laves phase is broken up into slabs".[29]

It has been emphasized[30] that "the Laves phases and the $CeCu_2$-Type polar intermetallics are competing structures realized for the same range of valence electrons, i.e., 6–8 electrons per formula unit, and that the boundary between open packed, polyanionic $CeCu_2$-typed phases and closed packed Laves phases is primarily governed by the electronegativity difference between the A and B component". Häusermann and others[30,31] have shown that $CeCu_2$-type polar intermetallics can be compressed into Laves phases. So, "high pressures have the effect of decreasing ΔEN", and this is in line with our observations pertaining to the development of charges in view of bonding in these systems.

Besides the hexagonal Laves phase (see Figure 10b) there is another polymorph of $MgAl_2$ (*I4$_1$/amd*) (see Table 1 and Figure 10c) where the average bond number is even higher. Its basin volumes and charges follow the general rules discussed above, there is a very distinct difference in charges (−0.35 and −1.09) between the two Al sites corresponding with the bond numbers (8 and 6), and the volume per atom is even slightly lower than for the Laves phase which may surprise since this form has been prepared by splat cooling techniques which normally favour disorder and defects. In this case the parameters "bond number" and "local polarity" act in the same direction producing the distinct difference of charge.

The Laves phase structures are retained on variation of the valence electron concentration within certain regimes when "blending" the appropriate compound with elements from lower or higher groups.[23,24] The three types of Laves phases ($MgCu_2$, $MgZn_2$ and $MgNi_2$) abound in binary intermetallics, and many ternaries or even quaternary variants are found which are only a sort of "colouring" of these arrangements with slight distortions.[32] We may state that the well-known textbook explanations given for the preference and for the stability of the Laves phases may in general be a helpful descriptive means to rationalize the existence of these compounds. However. in view of the findings presented here we must regret that they do not fill the need for a complete cause-and-effect-chain to explain the dominance of such a structural arrangement in this group of intermetallic compounds. In our opinion these Laves phases are not fully understood yet though they are almost omnipresent.

On the Development of Bond Nets

In the crystal structures of binary AE-TR-compounds we find variations of general patterns of bond nets which are due to different size relations of the atomic constituents. We see 3D-nets of bonded trielide atoms with the alkaline earth partners inserted into their cavities, and these nets are expanded or contracted depending on the relative sizes of the components in such a way that some of the bonded contacts are either lost or formed. This may nicely be described in a comparison of digallides as shown in Figure 11.

The AlB_2-type (a) is made up of flat Ca layers and honeycomb-type layers of Ga and – other than expected – with 3 bonds only to neighbouring atoms. In the $CaIn_2$-type structure (b) these layers are puckered, and this allows a closer packing (V/at 21.9 Å^3 vs. 23.4 Å^3). Since Mg is smaller than Ca these layers approach more in $MgGa_2$-I and a fourth bond bridging them can now additionally be formed (c). The $YCrB_4$-type (d) is a topological variant where 8-membered and 6-membered puckered rings alternate within the Ga layers which are now "welded together" via their opposite apexes in a crown-type configuration instead of the additional bridging contact in the

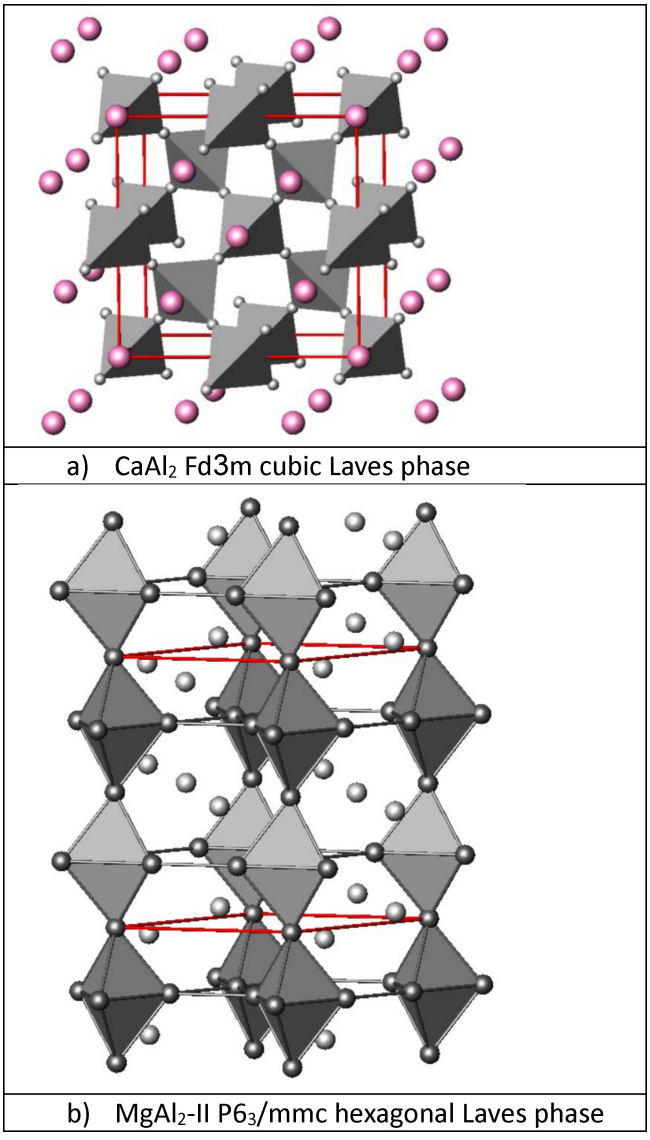

Figure 10. The structures of the cubic Laves phase ($CaAl_2$) (a) and of the two polymorphs of $MgAl_2$, the hexagonal Laves phase (*$P6_3/mmc$*) (b) and the $HfGa_2$-type (*$I4_1/amd$*) (c), Ca pink, Mg light grey, Al dark grey.

$CaIn_2$-type arrangement. The packing is now even slightly closer than in $MgGa_2$-I.

We may imagine a transition between these structures on dilating or compressing them, and indeed, such changes could occur in pressure or temperature induced polymorphic transformations.

We encounter a similar but even more complex situation when looking at some 1:1 compounds. In Figure 12 we compare examples derived from a CsCl-type arrangement with different bonding situations. To demonstrate the result of bonding of the trielide atoms in "movements" of the AE components we have highlighted their sublattices by dashed lines. There are no bonds in the high symmetry CsCl-type form of CaIn–I (a) but four bonds aligning the trielide atoms in a net of squares in the CuAu-type form of MgIn (b) where closer In–In contacts are possible. In the latter case this only results in a tetragonal distortion of the lattice, however, in the PuGa-type form of CaIn-II (c) we notice how the contraction into isolated squares with two bonds for each atom forces the Ca atoms above and below them to move away. The bonding features found in these CsCl-type related structures do not comply with our expectations since for these examples we should rather expect threefold bonded trielide atoms. We show the arrangement of the LiSi-type of MgGa for comparison (d) which follows a completely different and unique scheme. This example complies with our expectations. There are three-bonded Ga atoms forming screws which progress along [001].

As a last example we present structures derived from the anti-TlI- or CaSn-type arrangement where zig-zag chains of bonded atoms are the prominent feature. In these structures all atoms are coordinated by 6 neighbouring counterparts in the form of a trigonal prism. Since these prisms share two of their rectangular faces, the atoms at their centres are quite close and can interact by bond formation or by ns^2-ns^2-interaction as in TlI or related compounds. We compare the structures of CaGa, BaIn and SrIn in Figure 13 where we have again highlighted the sublattice of the AE atoms by dashed lines to demonstrate the

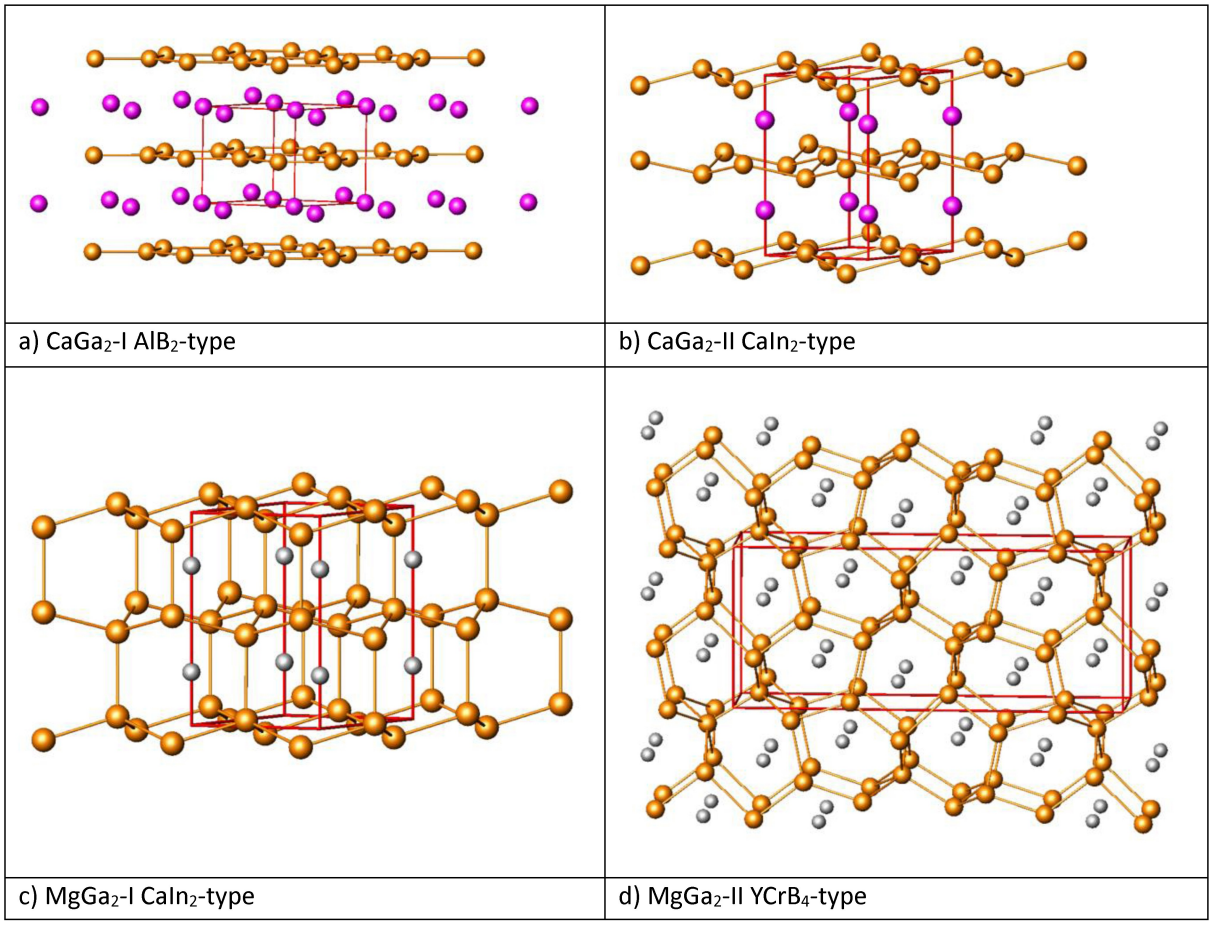

Figure 11. A comparison of digallides, a) $CaGa_2$-I (*P6/mmm*), b) $CaGa_2$-II (*P6$_3$/mmc*), c) $MgGa_2$-I (*P6$_3$/mmc*), d) $MgGa_2$-II (*Pbam*).

result of bonding of the trielide atoms in "movements" of the AE components.

In CaGa (Figure 13 a) we see isolated zig-zag chains of Ga running along [001] which is also the viewing direction. They are offset by $^1/_2$ a in neighbouring columns, so Ga and Ca atoms are assembled within the same (100) layers. Figure 13b shows BaIn in the same projection. Here we see Ba and In assembled in different (100) layers. The zig-zag chains of In have pairwise moved closer in [001] direction and this has forced the Ba atoms in between to move out. There are shorter and longer Ba–Ba contacts within the (100) layer. In comparison with CaGa the AE-sublattice is now distinctly deformed. Bonding in CaGa does not comply with our expectations, it does for BaIn where we now have three bonds just as in the last example shown in Figure 13 c. However, in SrIn the third bond is not realized by a pairwise association of chains as in BaIn. There is now an alternating contact for the In atoms of two In up and two down in [100] direction. The expansion of the Sr sublattice by localized In–In bonds is now more uniform than in BaIn with its double chains of In atoms. We now have slabs of Sr and In alternating in [001] direction to the right in this picture. As in CaGa we now see In chains and Sr atoms within the same (100) layer.

Group-Subgroup Relations

The examples given above nicely demonstrate how bond formation can lead to a deformation of an otherwise favoured structural matrix. Size relations between AE and TR atoms define whether the latter ones are kept apart or are close enough to combine. One could imagine dynamic changes between such different configurations and a closer inspection of polymorphic transitions under pressure or varying temperatures should reveal further examples of this kind which will then be classified as displacive polymorphic transitions. As a matter of course such structural relationships can also be documented by group-subgroup relations following the concise Bärnighausen formalism.[6,7]

We give two examples of this kind in the following where we present abbreviated Bärnighausen trees giving only the indices for the *klassengleiche (k)* and *translationengleiche (t)* symmetry reductions and the unit cell transformations. In some cases, a shift of origin is also noted down in square brackets. Further examples and extended trees along with the evolution of Wyckoff sites and atomic parameters are presented in the electronic supplementary information file (ESI).

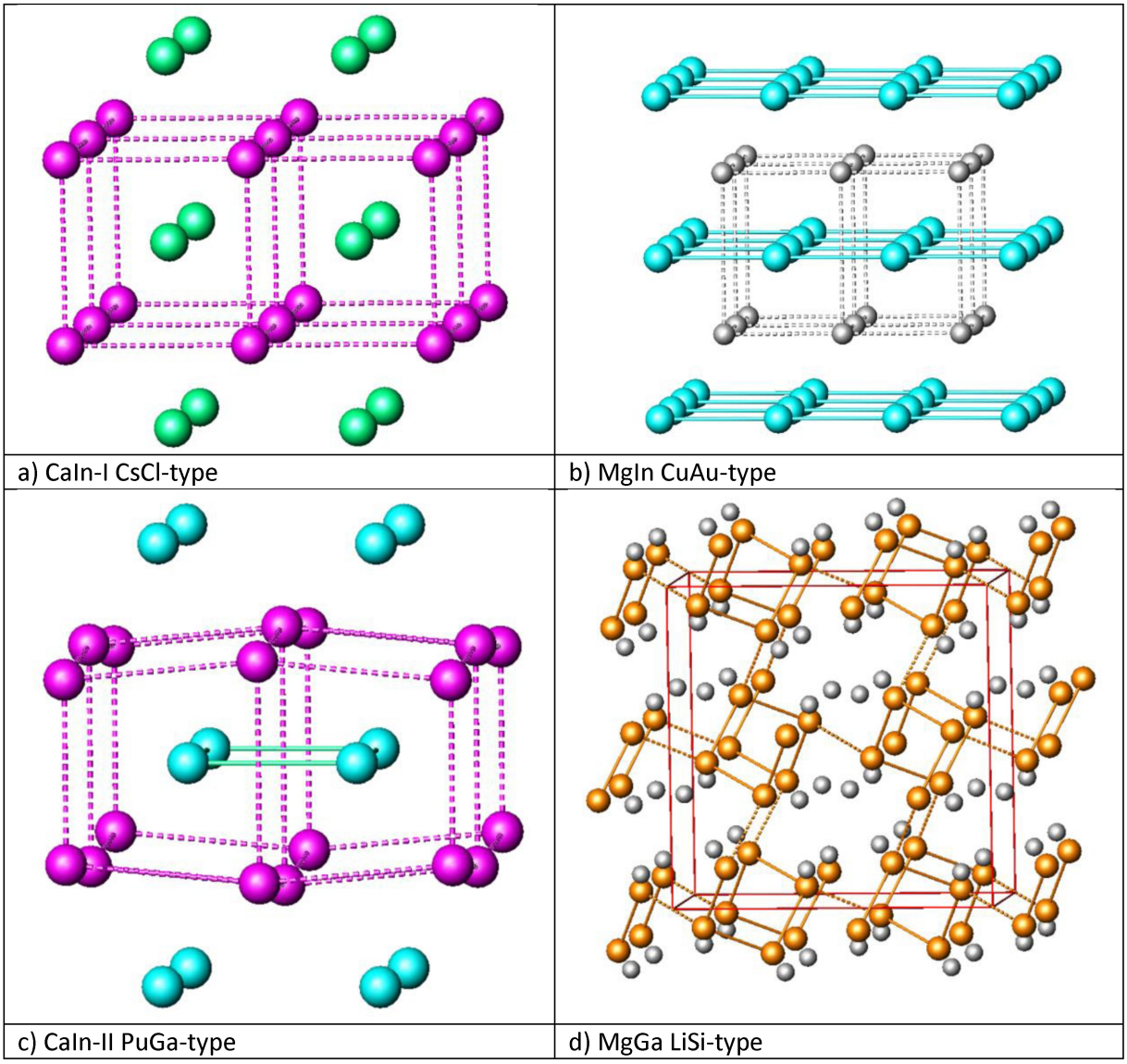

Figure 12. A comparison of mono-trielides with structures derived from the CsCl-type, a) CaIn ($Pm\bar{3}m$), b) MgIn ($P4/mmm$), c) CaIn-II ($I4/mmm$), d) MgGa ($I4_1/a$).

In a first scheme (Figure 14) we see three structure types in their group subgroup relations. The AlB_2 -type and the $CaIn_2$-type have been shown in Figure 11. We must also point out that – depending on the size relations of the constituent atoms – we find either 3 or 4 bonds for the trielide partners in the latter structure type. The fourth bond is realized as a link to the layers above and below alternating within the six-membered rings. To complete the pictures, we present a view along [0 1 0] of the KHg_2-type (or $CeCu_2$-type) as shown for $SrAl_2$-II in Figure 15. We again find zig-zag chains like in the TlI-type running along [0 1 0]. They are connected first in pairs like in the NaHg-type described above. Within the six-membered Al rings three of them link to the layer above and the next three to the layer below. The double zig-zag chains are thereby additionally attached to other ones forming puckered (0 1 0) planes. The alkaline earth atoms fill the cavities within the nets formed by the four-bonded Al atoms. We have again marked the cation sublattice by dashed lines to demonstrate how bond formation between the Al atoms deforms the parent Sr-substructure.

In the paragraph above we have presented relations between polymorphs of CaIn as an example for a 1:1 stoichiometric ratio where the high symmetry structure of CsCl is deformed by bond formation in the In sublattice. Figure 16 summarizes the group-subgroup relation between the two structures. In this example the pathway down the symmetry tree is slightly complicated by the need to change the origin and to comply with the conventions of the International Tables which avoid C- and F-centred space groups in the tetragonal system.

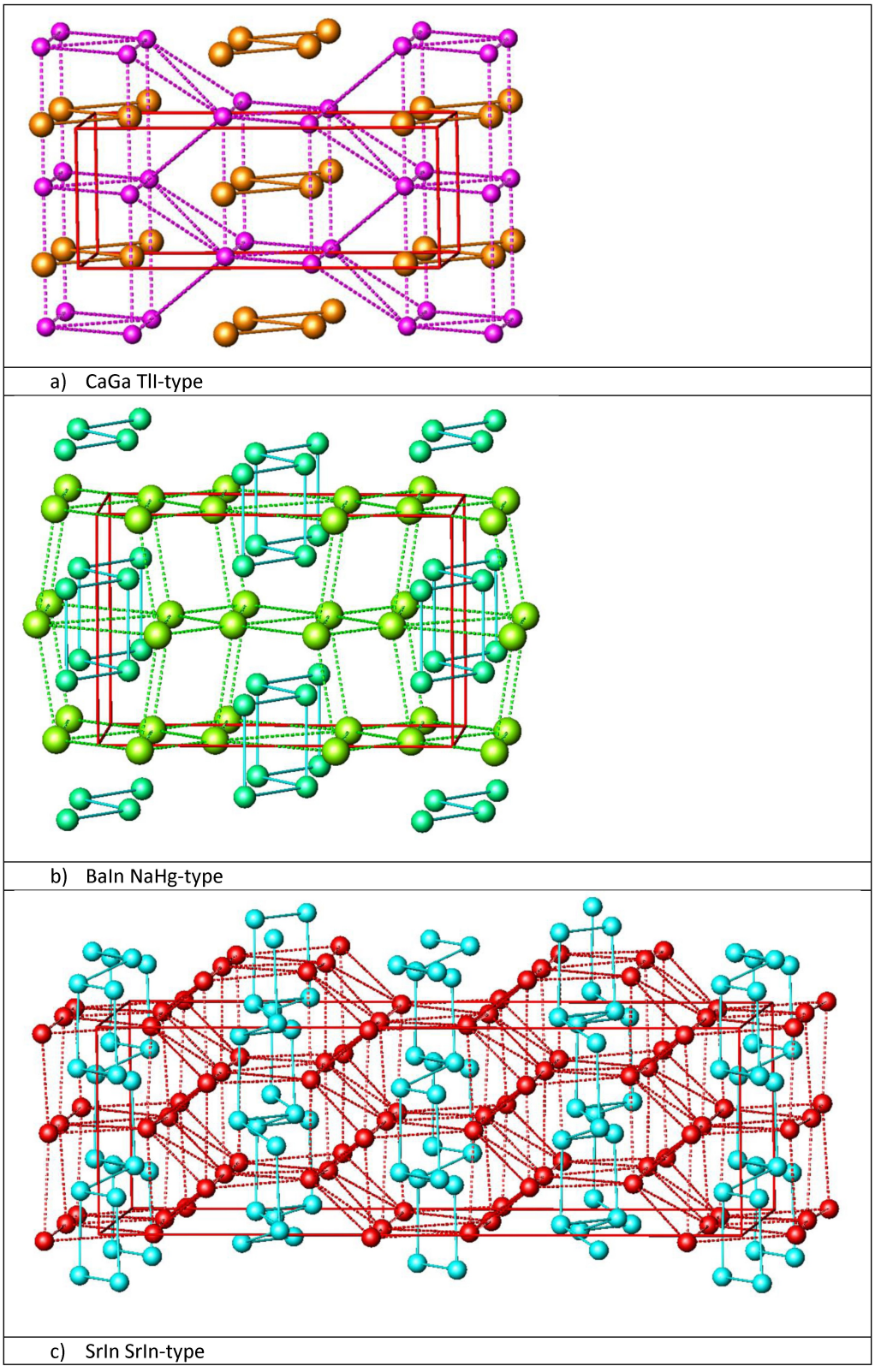

Figure 13. Structures derived from the TlI-type, a) CaGa (*Cmcm-I*), b) BaIn (*Cmcm-II*), c) SrIn (*Fdd2*).

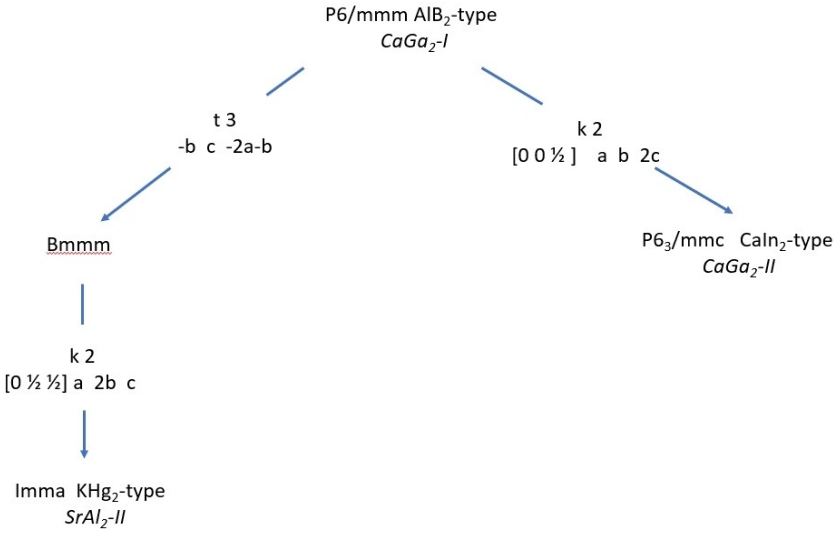

Figure 14. Group-subgroup scheme joining the structures of $CaGa_2$-I, $CaGa_2$-II and $SrAl_2$.

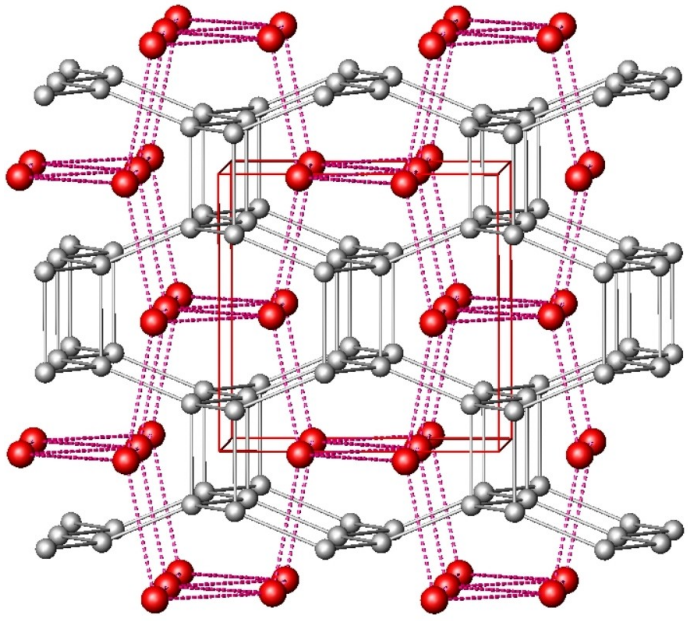

Figure 15. $SrAl_2$-II ($CeCu_2$ or KHg_2-type), view along [1 0 0].

Probing the Parameter Set for Hidden Correlations – a PCA Study

In the topological analysis of the structures of the AE_xTR_y binaries and in the DFT results we find characteristic features which we tend to explain in the frame of the Zintl concept. Due to clear interrelations between some of the resulting parameters we are tempted to see causal relationships and to derive rules or even laws to explain the formation of bonding nets and the stability of compounds. However, as stated above, we stumble over many misfits when bluntly trying to adopt Zintl-rules to explain the bonding situation in the structures of many compounds. We have therefore tried to examine the results of such analyses in more detail to quantify the strength of these correlations and to find "hidden" hints to set out "true" causal dependencies.

The set of parameters used for a principal component analysis (PCA) contains the mol fraction of the AE elements, the energies per atom, and then the average charges and basin volumes of the atoms together with the average bonding number of the trielide atoms. We have mentioned above that the formal number of electrons transferred is almost never realized in these compounds. We have therefore added the relation of the effective transfer (Bader charge of the trielide) to

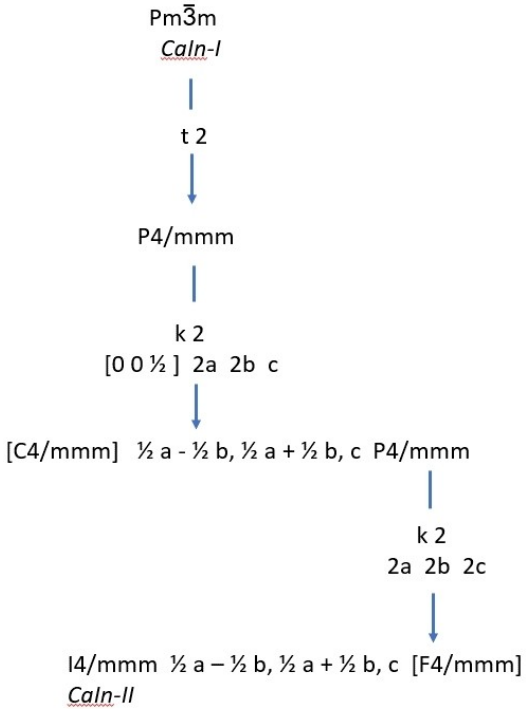

Figure 16. Group-subgroup scheme comparing the structures of CaIn–I and CaIn-II.

the formally possible one (2·x/y) as an additional average parameter (rel+/TR). The parameter rtbond describes the relation between the real and the expected bond number, and finally we include a weighted ΔEN ((EN(B)−EN(A))·x/y) to modify the electronegativity difference by the stoichiometric composition.

As a first result we may study the correlation r between these parameters defined – as is known – by

$$r = \frac{cov(x,y)}{S_x S_y}, \text{ where } cov(x,y) = \frac{\Sigma_{i=1}^{n}(x_i - \bar{x})(y_i - \bar{y})}{n-1} \text{ and}$$

$$S_x = \sqrt{\frac{\Sigma_{i=1}^{n}(x_i - \bar{x})^2}{n-1}}.$$

Table 6 (and Tables S5 to S7 in the ESI) give the correlation matrices of these parameters for trielides of Ca, Sr and Ba. (We have left out the Mg compounds which behave quite differently and – as stated above – are a class of their own.) For a better overview we have coloured these tables in the form of heat maps giving negative correlations in red and positive ones in green. The strength of these correlations is furthermore differentiated by the intensity of these colours, lighter colours mark weaker correlations. This allows a quick comparison to see that the matrices of the aluminides, gallides, indides and thallides are virtually similar – as they should – with respect to the distribution of positive and negative correlations. The only difference being the values of the correlation coefficients themselves. There are changes from highly to less correlated parameters and vice versa. In the following we focus first on the results for the aluminides.

We may compare these results with our expectations in relation to the Zintl concept. We do expect an increase of the negative charge of the trielide with increasing mol fraction of the AE component and hence an increase of its basin volume. The decrease of bonding by electron transfer with growing mol fraction is also a key message of the Zintl concept. The strong positive correlation of the energy per atom with its growing negative charge and consequently a negative correlation with the trielide basin volume is self-explaining as well since this reflects the effect of increasing polarity and hence growing Madelung contributions to the lattice energy. The strong negative correlation between AE charge and AE volume is trivial just as the positive connection between TR charge and volume. The observation that the charge of the trielide and its bonding number are strongly connected has been pointed out above as an important new finding in the Bader analyses, and finally, we see the influence of ΔEN on the energy per atom and on the parameters related with charge and basin volume of the TR component. Some correlation pairs seem puzzling at first sight. However, they do fit. Take the parameter rtbond and the charge and volume of Al with positive and negative correlation respectively as an example. More bonds (than expected) will "decrease the negative charge" (a positive effect!) and decrease the volume (a negative effect!).

There is some redundancy in this parameter set. However, it makes sense to keep all of them because when looking more closely we find some trends and significant changes in the intensity of colouring, i.e., in the degree of correlation, when moving down the trielide group from Al to Tl.

The AE mol fraction is highly correlated with the energy/atom for aluminides and gallides, but distinctly less for indides and thallides. There is an interesting connection between the "weighted" ΔEN and the parameter rel+/TR (deviation of the Bader charge from the theoretically possible electron transfer). Their (negative) correlation is negligible for aluminides but it becomes more and more important when changing to gallides, indides and finally thallides. Looking separately at these groups we see that this parameter decreases within each group when moving from Ca- to Ba-compounds. Even though ΔEN increases, the Bader charges miss the formally possible electron transfer more and more. A paradox situation not anticipated before which we have discussed above as a consequence of a growing misfit of the electronic energy states of the AE-TR partners!

Therefore, when making the same calculations with all binary trielide compounds in a combined set, the appearance of this correlation matrix changes distinctly (Table 6b). The colouring already shows that many correlations have become much weaker or have even disappeared completely. First, the different individual characters of the trielide elements sometimes lead to a different set of stoichiometric compositions in the combination with these alkaline earth elements (see Figure 1) giving different weights in the statistics, and second, the difference in EN and size is clearly reflected in many of the parameters in this correlation table. However, despite the

Table 6 Correlation matrices for trielides of the alkaline earth elements Ca, Sr and Ba (see text) (the ones for gallides, indides and thallides are presented in the electronic supplementary information, S5 to S7)

a) Correlation matrix for aluminides alone

	mfractAE	En/at	avAEcha	avAlcha	avAEvol	avAlvol	rele+/Tr	avbond	delENrel	rtbond
mfractAE	1	0,965	-0,355	-0,919	0,256	0,9	-0,361	-0,826	0,96	-0,693
En/at	0,965	1	-0,296	-0,896	0,261	0,924	-0,3	-0,867	0,949	-0,76
avAEcha	-0,355	-0,296	1	0,109	-0,908	-0,189	0,998	0,155	-0,283	0,062
avAlcha	-0,919	-0,896	0,109	1	0,002	-0,957	0,115	0,86	-0,978	0,816
avAEvol	0,256	0,261	-0,908	0,002	1	0,149	-0,901	-0,219	0,186	-0,126
avAlvol	0,9	0,924	-0,189	-0,957	0,149	1	-0,196	-0,881	0,974	-0,847
rele+/Tr	-0,361	-0,3	0,998	0,115	-0,901	-0,196	1	0,157	-0,289	0,061
avbond	-0,826	-0,867	0,155	0,86	-0,219	-0,881	0,157	1	-0,881	0,96
delENrel	0,96	0,949	-0,283	-0,978	0,186	0,974	-0,289	-0,881	1	-0,817
rtbond	-0,693	-0,76	0,062	0,816	-0,126	-0,848	0,061	0,96	-0,817	1

b) Correlation matrix for all AE/TR combinations

	mfractAE	En/at	avAEcha	avTRcha	avAEvol	avTrvol	rele+/Tr	avbond	delENrel	rtbond
mfractAE	1	0,587	-0,604	-0,947	0,227	0,901	-0,598	-0,819	0,941	-0,531
En/at	0,587	1	-0,202	-0,608	0,237	0,784	-0,197	-0,439	0,641	-0,215
avAEcha	-0,604	-0,202	1	0,468	-0,748	-0,485	0,997	0,444	-0,605	0,265
avTRcha	-0,947	-0,608	0,468	1	-0,081	-0,939	0,457	0,822	-0,959	0,556
avAEvol	0,227	0,237	-0,748	-0,081	1	0,246	-0,746	-0,187	0,251	-0,148
avTrvol	0,901	0,784	-0,485	-0,939	0,246	1	-0,473	-0,772	0,941	-0,517
rele+/Tr	-0,598	-0,197	0,997	0,457	-0,746	-0,473	1	0,436	-0,596	0,251
avbond	-0,819	-0,439	0,444	0,822	-0,187	-0,772	0,436	1	-0,820	0,857
delENrel	0,941	0,641	-0,605	-0,959	0,251	0,941	-0,596	-0,820	1	-0,531
rtbond	-0,531	-0,215	0,265	0,556	-0,148	-0,518	0,251	0,857	-0,531	1

strong heterogeneity in this set some characteristics coherent with the Zintl concept are retained throughout all compounds.

All in all, we see a complex net of stronger and weaker correlations most of which match our expectations, but there are also some non-trivial combinations which we might not have expected. It was therefore interesting to see all results of the multivariate statistics. A pictorial presentation of such correlations is given in the customary "biplot" where the orientations in a multidimensional space of fictitious "principal components" of different kinds of parameters (loadings) are given as vectors and the position of the compounds in this space as coordinates (scores). In all our sets of alkaline earth trielides the first three principal components (PCs) cover around 90 % of the total variance information, so, it may suffice to study only these three dimensions. In Figure 17 a, b we present biplots for aluminides showing scores and loadings together in a projection onto the PC1/PC2 and the PC1/PC3 plane to give an impression of the spread of these parameters in the 3-dimensional space defined by these three most important principal components. The percentages given along the axes define the contribution of the respective PC to the whole data set. We again start with the aluminides alone.

In Figure 17 a) we find the Ca-, Sr- and Ba-compounds grouped in clusters within different regions in this space which we may envisage as a three-axed ellipsoid of which we see only the projection onto the PC1/PC2 plane. The respective graphs for gallides, indides and thallides have a similar appearance. The first PC is defined by a mixture of loadings among which the mol fraction of AE is especially prominent. We therefore find the compounds within their clusters assembled mostly along the PC1 direction according to the AE content. Other parameters which correlate strongly with the mol fraction

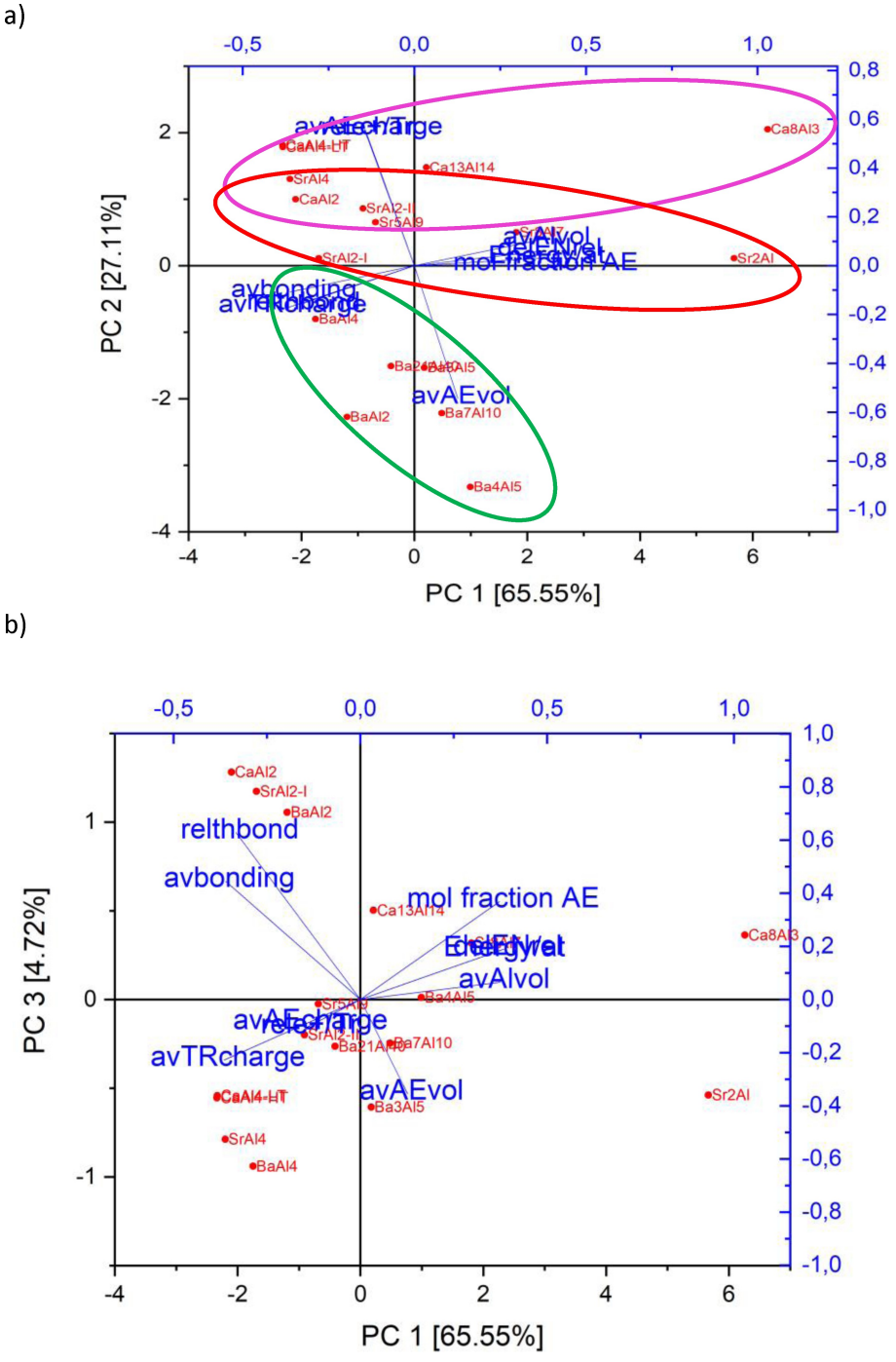

Figure 17. a) PC1/PC2 and b) PC1/PC3 projection of loadings and scores of Ca-, Sr- and Ba-aluminides (see text!).

according to the table given above, e.g., the deviation of Bader charges from the possible transfer numbers, also line up along this direction. The clusters of the Ca-, Sr- and Ba compounds are spread along the PC2 direction which is dominated by the charge and volume parameters of the cation species of the different compounds, and as a prominent feature in the PC3 direction we find the vector of the average bonding number of the trielide and the cation charge in almost opposite direction. The angles between the loadings' vectors depict the degree of correlation between these parameters. They are positively correlated for small angles, independent when standing orthogonally and have an increasing negative correlation for angles growing beyond 90°. The high negative correlation between the AE mol fraction and these cation parameters end up in the respective loading vectors pointing away from each other. The same is true for the pair molfraction/Alcharge which is strongly anti-correlated as discussed above. The angle between the mol fraction and the average bonding number –

both located mostly in the PC1/PC3 plane – is about 77°, not far from an orthogonal relation, and this demonstrates once again that Zintl counting rules contribute distinctly less than expected to the bonding topology in our structures.

In Figure 18 a, b we give the biplots resulting from a calculation including all binary compounds together in one set, i.e. the pictorial representation of the Table 6b.

Though many correlations are weaker – as documented in a comparison of Tables 6a and 6 b – the pictures are quite similar. The mol fraction together with all other parameters derived from them dominate PC1 and size relations of the alkaline earth atoms are clearly reflected in the PC2 direction.

Borderline Cases

To come back to a more conventional view Figure 19 presents a comparison between the average bond numbers found for compounds in this study and the relative deviation from the theoretically expected ones according to a simple Zintl counting scheme. (A perfect fit would be represented by the relation real/theobond = 1.)

We find a considerable number of examples where the real bond numbers are below as well as above our expectations. Bond numbers around 4 rather meet them (real/theobond ≈ 1.0), in other cases the deviations can be quite large. It is interesting to note that lower average bond numbers are

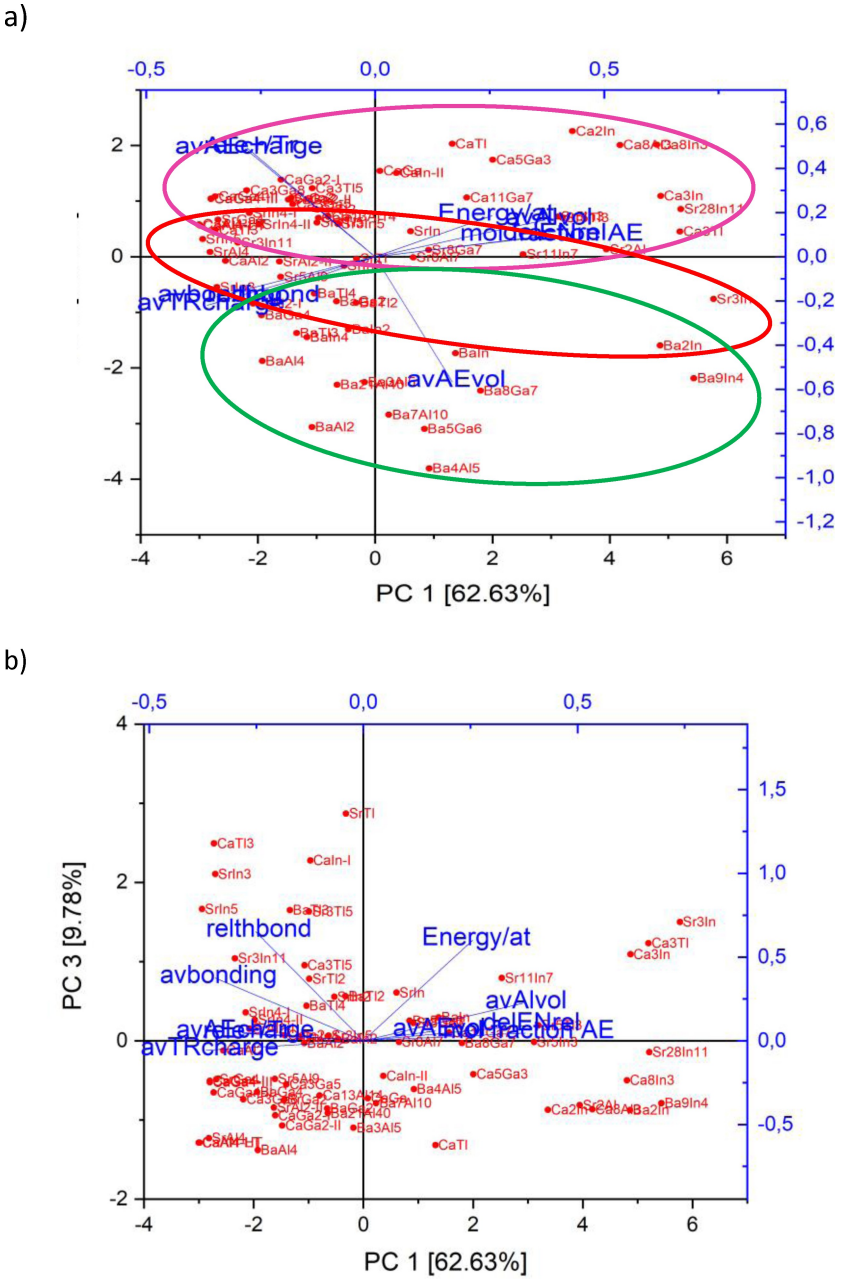

Figure 18. a) PC1/PC2 and b) PC1/PC3 projection of loadings and scores of all binary trielides (see text!).

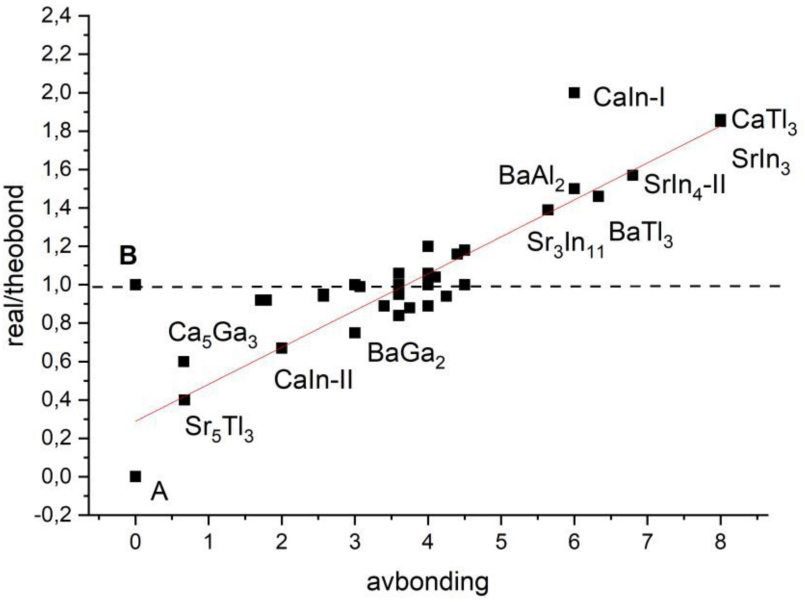

Figure 19. Real bond numbers for all compounds as tabulated in Tables 1–4 in relation to theoretically expected ones according to the Zintl counting rule, A examples with no bonds though some are expected, B examples with zero bonds as expected.

mostly below and higher bond numbers mostly above our expectations. The transfer of many electrons to spawn ψ-chalcogenides or even ψ -halides is rarely achieved, in contrast, the formation of more bonds to compensate for too little electron transfer is seen quite often.

This can be summarized in a general statement. First, we have noticed that there is a mechanism to avoid the transfer of too many electrons even when the stoichiometric relations and the electronegativity difference would favour it, and second, the formation of bonds is often preferred instead, and this reduces the charge on the trielide atoms.

The term 2x/y in the Zintl counting equation cannot exceed 5 for simple reasons, compounds like Mg_5In_2 are borderline examples in this game with In acting as "ψ-Xe". As expected, we find a typical coordination structure for $Mg_5^{[4]}In_2^{[10]}$ with isolated and highly coordinated In atoms, contra wise Sr_5Tl_3 should have a mixture of double-bonded and single-bonded Tl atoms but we see only zero- and single-bonded ones. Ca_3Tl and similar compounds have Heusler-type (Figure 20c) or $AuCu_3$-type (Figure 20d) structures, which are all reminiscent of structures found for elements like Ga or In and for typical structures of metals and alloys including borides where multi-centre bonding abounds. The expected electron transfer is partly blocked avoiding higher bond numbers, and this is documented in the positive correlation between the average bond number itself and its deviation from the theoretical one.

On the other side of this scale, we find a borderline example with the $BaAl_4$-type structure where – as stated above – some of the trielide atoms are hosted in a metal-like situation. In other cases, very small electron contributions of the AE partners like in $SrIn_3$ (see Figure 20 a) or Sr_3In_{11} (see Figure 20 b) result in trielide clustering in two or three dimensions. So, in a way, the lack of electrons is compensated by stronger bonding! The two extremes interplay in an opposite way to avoid deficiencies or abundances.

Summary

The binary compounds of the alkaline earth trielides have proven to be an interesting group of compounds to study the validity of the Zintl concept. The results of DFT calculations of about 90 members of this group have been assembled in tables giving the calculated cell parameters, the energies per atom and the Bader charges and basin volumes of all atoms at their respective Wyckoff sites. In a first run all these data have helped to estimate the energies of formation and the stability of the compounds by a discussion of hull curves. This has shown up similarities as well as distinct differences of the different alkaline earth trielides. There are general trends in the hull curves giving the formation enthalpies. The convex nature of these curves increases when going down the AE group from Mg to Ba for all trielides respectively. The formation enthalpy is negligible or small for Mg compounds, and it increases on going down the AE group. So, the electropositive nature of the alkaline earth is very important and the polarity, i.e., the electrostatic contribution to the overall lattice energy plays a decisive role for the stability of these compounds.

An important finding comes up in the comparison of Bader charges and bond formation. The variation of charges for atoms at different Wyckoff sites was studied in more detail. First, the charges of the trielide atoms decrease with increasing number of bonds they form with each other, and second, a finer scaling among such charges can be rationalized in a detailed study of the environments of the respective trielide atoms.

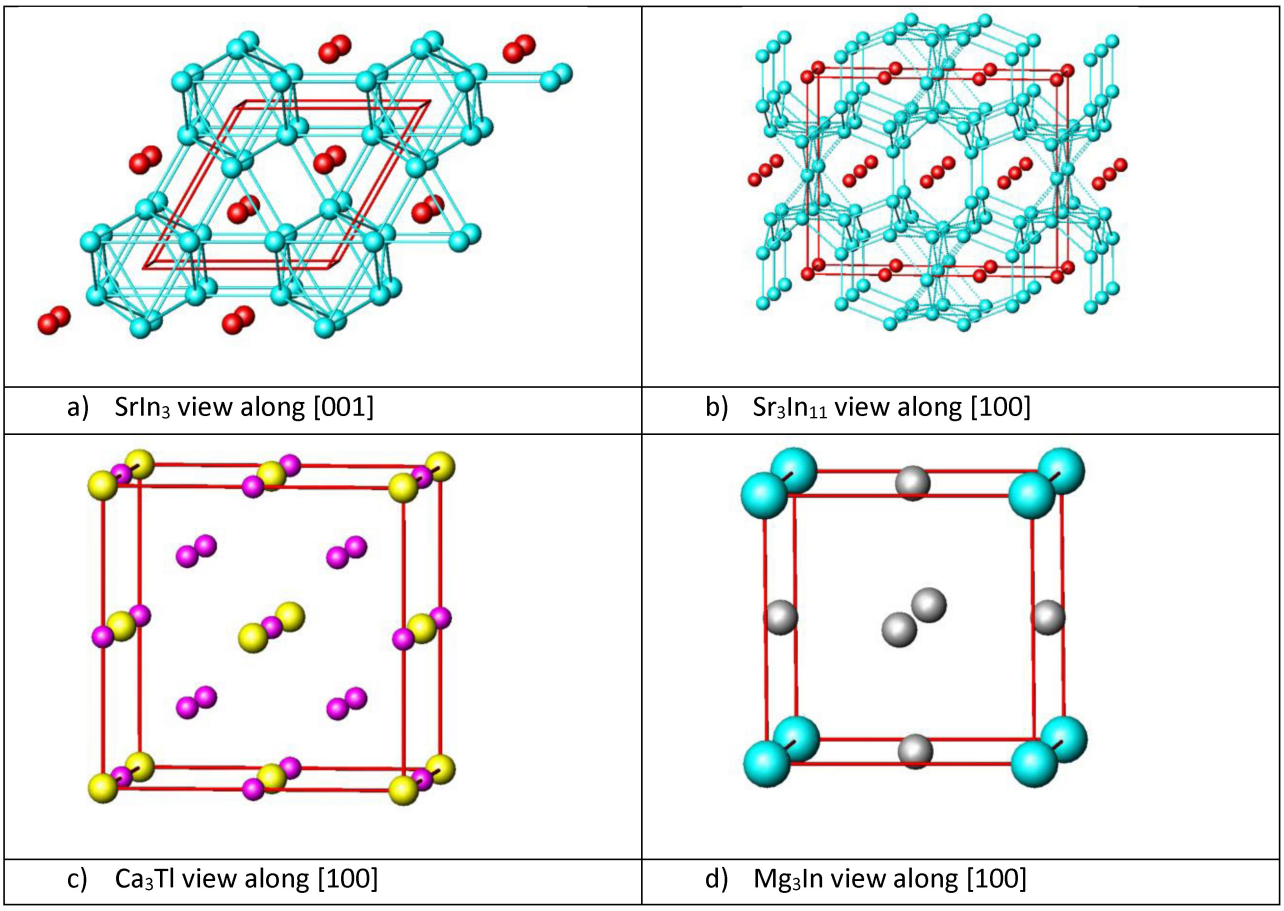

Figure 20. Examples for very small [(a)$SrIn_3$ or (b) Sr_3In_{11}] and high [(c) Ca_3Tl or (d) Mg_3In] electron contributions of AE to TR-TR bonding nets.

The resulting set of bonding was studied in relation to the expectations of the Zintl concept. It becomes evident that the theoretical electron transfers according to the electronegativity relationship and the corresponding bond formation according to this concept cannot be expressed as a rule but rather as a "frequent result". We may state generally that there is a mechanism to avoid the transfer of many electrons even when the stoichiometric relations and the electronegativity difference would favour it, and second, the formation of bonds is often preferred instead, and this reduces the charge on the trielide atoms. So, bond numbers will very often not be consistent with our expectations, and for cases with very low electron transfer we find typical alloy topologies such as Heusler structures or AuCu- and $AuCu_3$-type arrangements.

A fundamental deviation from our expectations according to the Zintl concept is found in the form of the Laves phases. These structures very often occur for binary intermetallics and then also in "coloured forms" in ternary and quaternary variants. They have been described in detail in textbooks together with many "explanations" for their existence, such as size-relations and valence electron concentrations. However, they are outlaws in the world of Zintl compounds insofar as they neither follow its rules, nor do they follow the evolution of other parameters which we have found to be typical for the "real" Zintl phases.

The topology of bond nets in these trielides is a topic of its own. We find singular geometries for specific stoichiometries and element combinations but also some widespread examples. Typical structures and bonding nets are found for 1:1, 1:2, 1:4, 2:1 and 3:1 compounds among the AE_xTR_y set. We see nets of bonded TR-atoms with cavities into which the AE components are embedded, and depending on the size of the alkaline earth partner these nets are widened or contracted so that some bonds are cleaved or formed. We have trailed some of these topological evolutions with the concomitant symmetry reductions in the form of Bärnighausen trees showing the stepwise decrease of site symmetries in the space groups.

The tables compiled in this work offer many parameters such as individual charges, basin sizes of the atoms, total energies of all compounds and others. We have hoped to find hidden correlations giving some deeper insights into the mechanisms governing the formation and the resulting structures by probing this complex data set by a statistic multivariate analysis. In addition to the parameters mentioned we have included a "weighted" ΔEN and deviations from the "expected" electron transfer on the one hand and of the deviations from

the expected bond numbers as well on the other hand to analyse their "connection" to other parameters. We understand that correlations are not causes, but we hoped to find some help to rationalize criteria for the validity or failure of the Zintl concept in this class of compounds.

We have depicted the relationship between all these parameters in the form of correlation matrices coloured as heat maps and then also in the form of biplots as used in principal component analysis (PCA). Many correlations turn out to be trivial, but some others may surprise. As expected, the mol fraction of the AE component is a dominant factor as shown by its correlation with average TR charges and basin volumes for all elemental combinations. However, its impact on the average bonding number is distinctly weaker, it is still strongest for gallides and indides, but weakest for thallides. We also realize from the correlation matrices that increasing bond numbers lead to a reduction of the negative charge of the trielide atoms. First, bonding counteracts the amount of electron transfer which would be expected according to electronegativity differences of the partners, and second, even though ΔEN increases in iso-stoichiometric series, the Bader charges miss the formally possible electron transfer more and more when going down the AE group from Mg to Ba. A paradox situation not anticipated before! We may interpret this by a growing misfit of atomic energy states or differences in the corresponding band energies for the AE-TR pairs when going down the trielide group in the periodic table.

Another, perhaps surprising result in the search for interdependencies is the observation of an almost linear correlation between the average bond numbers and the deviation from the expected numbers according to the Zintl concept. High bond numbers – because of very little electron transfer – tend to be higher than expected, and low bond numbers – resulting from much electron transfer – are mostly lower than expected. We observe that in these extreme situations of electron deficiency or abundancy the mechanism of bond formation is active in a divergent way by increasing or reducing bond numbers respectively.

When comparing the "coloured" correlation matrices for the individual trielides and the one in which the total set is combined we see that correlations in the latter have become much weaker or have even disappeared completely due to the different properties of the elements. The trielide elements are by far not so uniform as the alkaline earth partners. However, despite the strong heterogeneity in this set some characteristics coherent with the Zintl concept are retained throughout all compounds.

Acknowledgements

Open Access funding enabled and organized by Projekt DEAL.

Conflict of Interest

The author declares no conflict of interest.

Data Availability Statement

The data that support the findings of this study are available in the supplementary material of this article.

Keywords: Zintl concept · Hull curves · DFT calculations · Bader analysis · Principal Component Analysis (PCA)

[1] J. D. Corbett, *Angew. Chem. Int. Ed.* **2000**, *39*, 670.
[2] J. D. Corbett, in S. M. Kauzlarich (Ed.), *Chemistry, Structure and Bonding of Zintl phases and ions*, VCH, New York, **1996**, pp. 139–181.
[3] C. Cordier, B. Eisenmann, in S. M. Kauzlarich (Ed.), *Chemistry, Structure and Bonding of Zintl phases and ions*, VCH, New York, **1996**, pp.61–137.
[4] a) P. Villars, K. Cenzual, *Pearson's Crystal Data: Crystal Structure Database for Inorganic Compounds*, ASM International®, Materials Park, Ohio, USA **2023**; b) NIST Inorganic Crystal Structure Database, *NIST Standard Reference Database Number 3*, National Institute of Standards and Technology, Gaithersburg MD, 20899.
[5] COUPOT, T. G. Beyer, *A FORTRAN programme for the calculation of lattice energies and potentials*, Saarland University, 1996.
[6] H. Bärnighausen, *MATCH, Commun. Math. Chem.* **1980**, *9*,130–175.
[7] U. Müller, *Symmetry Relationships between Crystal Structures, Oxford University Press*, **2013**.
[8] P. E. Blochl, *Phys. Rev. B: Condens. Matter Mater. Phys.* **1994**, *50*, 17953–17979.
[9] G. Kresse, D. Joubert, *Phys. Rev. B: Condens. Matter Mater. Phys.* **1999**, *59*, 1758–1775.
[10] G. Kresse, J. Furthmüller, *Phys. Rev. B: Condens. Matter Mater. Phys.* **1996**, *54*, 11169–11186.
[11] G. Kresse, J. Furthmüller, *Comput. Mater. Sci.* **1996**, *6*, 15–50.
[12] J. P. Perdew, K. Burke, M. Ernzerhof, *Phys. Rev. Lett.* **1996**, *77*, 3865–3868.
[13] E. Sanville, S. D. Kenny, R. Smith, G. Henkelman, *J. Comput. Chem.* **2007**, *28*, 899–908.
[14] G. Henkelman, A. Arnaldsson, H. Jonsson, *Comput. Mater. Sci.* **2006**, *36*, 354–360.
[15] W. Tang, E. Sanville, G. Henkelman, *J. Phys. Condens. Matter* **2009**, *21*, 084204.
[16] M. L. Formasini, *Acta Crystallogr. Sect. C* **1983**, *39*,943–946.
[17] M. Jehle, H. Scherer, M. Wendorff, C. Röhr, *J. Solid State Chem.* **2009**, *182*, 1129–1135.
[18] A. A. Emery, C. Wolverton, *Sci. Data* **2017**,*4*, 170153.
[19] J. L. Murray, *Bull. Alloy Phase Diagrams* **1982**, *3*(1), 60–74.
[20] K. Ozturk, Y. Zhong, L.-Q. Chen, C. Wolverton, J. O. Sofo, Z.-K. Liu, *Metallurgical and Materials Transactions A* **2005**, *36A*, 5–13.
[21] H. Okamoto, *J. Phase Equilib. Diffus.* **2005**, *26*(4), 394.
[22] R. P. Elliot, F. A. Shunk, *Bull. Alloy Phase Diagrams* **1981**, *2*(3), 351–353.
[23] U. Häussermann, S. Amerioun, L. Eriksson, C.-S. Lee, G. J. Miller, *J. Am. Chem. Soc.* **2002**, *124*, 4371–4383.
[24] W. Harms, M. Wendorff, C. Röhr, *J. Alloys Compd.* **2009**, *469*, 89–101.
[25] D.-K. Seo, J. D. Corbett, *J. Am. Chem. Soc.* **2000**, *40*, 9621–9627.
[26] A. Otero-de-la-Roza, M. A. Blanco, A. Martin Pendas, V. Luana, *Comput. Phys. Commun.* **2009**, *180*, 157–166.
[27] H. Bhatia, A. G. Gyulassy, V. Lordi, J. AE. Pask, V. Pascucci, P.-T. Bremer, *J. Comput. Chem.* **2018**, *39*(16), 936–952.
[28] a) J. K. Burdett, G. J. Miller, *J. Chem. Mater.* **1990**, *2*, 12; b) M. Wendorff, C. Röhr, *Z. Anorg. Allg. Chem.* **2005**, *631*, 338.

[29] S. Amerioun, T. Yokosawa, S. Lidin, U. Häussermann, *Inorg. Chem.* **2004**, *43*, 4751–4760.
[30] S. Kal, E. Stoyanov, J.-P. Belieres, T. L. Groy, R. Norrestam, U. Häussermann, *Journal of Solid State Chemistry* **2008**, *181*, 3016–3023.
[31] G. Cordier, E. Czech, H. Schäfer *Z. Naturforsch.* **1982**, *37b*, 1442–1445.
[32] E. C. J. Gießelmann, R. Pöttgen, O. Janka, *Z. Anorg. Chem.* **2023**, *649*.
[33] A.-B. V. Mudring, J. D. Corbett, *J. Am. Chem. Soc.* **2004**, *126*, 5277.

Manuscript received: January 20, 2024
Revised manuscript received: March 3, 2024
Accepted manuscript online: March 12, 2024

